LOW TEMPERATURE CHEMICAL VAPOR DEPOSITION OF ZIRCONIUM NITRIDE IN A FLUIDIZED BED

A Thesis

by

MARIE ARRIETA

Submitted to the Office of Graduate Studies of
Texas A&M University
in partial fulfillment of the requirements for the degree of

MASTER OF SCIENCE

August 2012

Major Subject: Nuclear Engineering

Low Temperature Chemical Vapor Deposition of Zirconium Nitride in a Fluidized Bed

LOW TEMPERATURE CHEMICAL VAPOR DEPOSITION OF ZIRCONIUM NITRIDE IN A FLUIDIZED BED

A Thesis

by

MARIE ARRIETA

Submitted to the Office of Graduate Studies of
Texas A&M University
in partial fulfillment of the requirements for the degree of

MASTER OF SCIENCE

Approved by:

Chair of Committee,	Sean McDeavitt
Committee Members,	Delia Perez-Nunez
	Raymundo Arroyave
Head of Department,	Yassin Hassan

August 2012

Major Subject: Nuclear Engineering

ABSTRACT

Low Temperature Chemical Vapor Deposition of Zirconium Nitride in a Fluidized Bed.

(August 2012)

Marie Arrieta, B.S., University of New Mexico

Chair of Advisory Committee: Dr. Sean McDeavitt

The objective of this research was to design, assemble, and demonstrate the initial performance of a fluidized bed chemical vapor deposition (FB-CVD) system capable of producing thin, uniform zirconium nitride (ZrN) coatings (1 to 10 μm thick) on uranium-molybdenum (UMo) particulate fuel. Plate-type fuel with U-*x*Mo (*x* = 3 to 10 wt.%) particle fuel dispersed in an aluminum matrix is under development at Idaho National Laboratory (INL) for the Reduced Enrichment for Research and Test Reactors (RERTR) program. Initial irradiation tests performed at INL in the Advanced Test Reactor (ATR) indicate an interaction layer forms between the fuel microspheres and the matrix at relatively high power levels. These power levels induce higher temperatures which enables uranium diffusion into the aluminum during irradiation, eventually causing fuel plate failure. The objective of this work was to create a process to mitigate the fuel/matrix interaction by forming a thin barrier coating on the surface of the U-*x*Mo microspheres before incorporation into the dispersion fuel plate matrix.

One of the main challenges in performance of the FB-CVD system was the effective fluidization of a powder whose physical characteristics (size, density) are

continuously changing. To address this, two types of fluidized bed reaction vessels were designed and improved over the course of this research: a spouted fluidized bed and an inverted fluidized bed. Both reaction vessels utilized tetrakis(dimethylamino)zirconium (TDMAZ) and ammonia gas as precursors at atmospheric pressure. Tungsten wires and zirconia–silica (ZrO_2-SiO_2) microspheres were used as the substrates for the coating experiments. The substrate temperature and precursor gas flow were manipulated as the process variables.

The FB-CVD system was successful in forming zirconium based coatings on surrogate microspheres with elevated levels of chemical impurities. At atmospheric pressure, coatings of thicknesses ranging from 0.5μm to 1.5μm were produced between temperatures of 250°C and 350°C. The deposited coatings were characterized using scanning electron microscopy, energy dispersive spectroscopy and wavelength dispersive spectroscopy.

DEDICATION

This thesis is dedicated to my husband, Robert Arrieta, and my son, Diego Arrieta, I could not have come this far without you.

ACKNOWLEDGEMENTS

I would like to thank my committee chair, Dr. Sean McDeavitt for his patience and support, and for allowing me to take over the white board in his office with my thoughts and ideas throughout the course of this research. Thank you to my committee members, Dr. Delia Perez-Nunez and Dr. Raymundo Arroyave for their time and attention to detail.

I would like to acknowledge Sandia National Laboratories for awarding me the Master's Fellowship Award. I would like to especially acknowledge and extend my gratitude to my manager, Dr. Mark Ekman, and my mentors Janet Ahrens and Wendy Friedt, whose constant encouragement, guidance, and technical critique over the last two years proved invaluable.

I thank my friends and colleagues in the Fuel Cycle and Materials Laboratory, Carissa Humrickhouse-Helmreich, Grant Helmreich, Jeffrey Clemens, Chad Thompson and Chad Garcia for their willingness to discuss research ideas. A special thanks to Adam Parkinson for his excellent advice and innovative ideas. I would also like to thank Dr. Ray Guillemette (Geology and Geophysics Department, TAMU) for his expert assistance with SEM imaging and analysis and Bill Merka (Chemistry Department, TAMU) for his innovative ideas and expertise in working with glassware.

I would like to acknowledge Idaho National Laboratories and Drs. Dennis Keiser and Dan Wachs for supporting this project.

Finally, thanks to my mother, Valerie Valdez, and mother-in-law, Maria Prindle-Arrieta, for all of their help and encouragement and to my husband, Robert Arrieta, for his endless patience and love.

NOMENCLATURE

ATR	Advanced Test Reactor
CVD	Chemical Vapor Deposition
EPMA	Electron Probe Micro-Analyzer
PVD	Physical Vapor Deposition
DOE	Department of Energy
EDS	Energy Dispersive Spectroscopy
FB	Fluidized Bed
INL	Idaho National Laboratory
RERTR	Reduced Enrichment for Research and Test Reactors
SEM	Scanning Electron Microscope
TAMU	Texas A&M University
TDMAZ	Tetrakis (dimethylamino) Zirconium
WDS	Wavelength Dispersive Spectroscopy
ZrN	Zirconium Nitride

TABLE OF CONTENTS

Page

LIST OF FIGURES

FIGURE Page

FIGURE Page

FIGURE Page

LIST OF TABLES

1. INTRODUCTION

A fluidized bed chemical vapor deposition (FB-CVD) system was created to produce thin zirconium nitride coatings on particulate uranium-molybdenum fuel as part of the Reduced Enrichment for Research and Test Reactors (RERTR) program. The atmospheric pressure FB-CVD system was designed as a continuous flow system using the chemical precursors, ammonia and tetrakis(dimethylamido)zirconium (TDMAZ), along with argon gas in a hot wall reactor between the temperatures of 200°C and 350°C. The FB-CVD system evolved over the course of this research; three reaction vessel designs were tested and a total of twelve coating experiments were completed as the process variables were improved. The FB-CVD system was successful in forming zirconium based coatings on surrogate microspheres with varied levels of chemical impurities. Further optimization of the system components and process variables is continuing but this document describes the establishment of the FB-CVD system and processing procedures, and the nature of the initial coatings.

The United States was the first country to artificially enrich uranium. Following the Atoms for Peace Initiative in 1953, the United States began to annually export about 700 kilograms of highly enriched uranium (HEU) for use in research reactors [1-2], HEU refers to uranium with greater than 20 wt.% U-235.

This thesis follows the style of Journal of Nuclear Materials.

Growing nuclear terrorism concerns prompted by the potential proliferation of U.S. distributed HEU brought about the creation of the RERTR program in 1978. The mission of the RERTR program is to eliminate the use of HEU in civilian facilities worldwide; this goal is to be accomplished by developing advanced technology to enable the conversion of fuel utilized in research and test reactors from HEU to low enriched uranium (LEU); LEU refers to uranium with less than 20wt.% U-235 [1-4].

In 1978, the main types of fuels used by US designed, high flux density reactors were plate-type dispersion fuels. These fuel plates consisted of uranium-aluminum or U_3O_8 particle fuel, enriched to 93 wt.% U-235, dispersed in an aluminum matrix [2]. Conversion of these fuel plates from HEU to LEU requires either an increased uranium density in the fuel particles or an increased fuel loading in the aluminum plates to compensate for the lower enrichment and to meet the high flux demands of individual reactors. The practical commercial processing restriction of fuel particle volume loading in the plates, roughly 55 vol%, requires the increase of the uranium density in the fuel to above 14.5 g U/cc [2]. Pure uranium metal has the highest fissile density of the potential fuel candidates, but it exists in different phases over the different irradiation temperatures. At lower temperatures, the alpha phase of uranium has an orthorhombic structure and exhibits high anisotropic growth rate and swelling under irradiation. The high temperature γ phase of uranium has stable irradiation behavior, but the phase is thermodynamically unstable at room temperature. To stabilize the γ phase, uranium must be alloyed with other elements [2, 3, 6].

Several elements were identified that will form a solid solution with γ-uranium and also retain the γ-uranium as a metastable phase after cooling. A compromise between the solubility of the elements and the amount of each required to retain the 100% γ-phase of uranium led to the choice of molybdenum [3]. The uranium molybdenum alloy, with 7 wt.% molybdenum (U-7Mo), has a uranium density of 16.2 g U/cc, making it a candidate fuel for this program [4].

Initial irradiation tests completed at the Advanced Test Reactor (ATR) at Idaho National Laboratories (INL) demonstrated the U-7Mo alloys display stable behavior with low swelling at low irradiation temperatures [2]. At increased reactor power levels and fuel temperatures, inter-diffusion between the uranium and aluminum creates an interaction layer of UAl_2 and UAl_3 between the U-7Mo alloy and the aluminum matrix [2]. The UAl_x interaction layer has a lower thermal conductivity than that of the U-Mo alloy, which causes a temperature rise in the fuel. The temperature rise increases the interaction layer growth rate, and at higher temperatures and fuel burnup the aluminum matrix is almost completely consumed by the layer [2, 6]. The lower viscosity of the interaction layer contributes to volume expansion in the fuel as the fission gases will migrate through the fuel to the layer interface where relatively large pores can develop. The pores coalesce into large bubbles, in some cases resulting in eventual fuel plate failure [2, 6].

To address this challenge, a diffusion barrier coating around the U-7Mo microspheres is proposed to mitigate the interaction between the uranium fuel and the aluminum matrix [7, 8].

An effective diffusion barrier will be inert with respect to the materials it is interposed between, have good adhesion characteristics, high thermal conductivity and thermal stability, and will have uniform thickness and structure across the surface [9]. In addition, the barrier must be compatible with other production steps involved with the creation of the coated material and must be able to be reliably reproduced on a commercial scale. Mononitrides of zirconium, hafnium, and titanium fall into this category and have high thermal conductivity, low diffusivity, and high melting points [9]. Mononitrides of zirconium and titanium are of particular interest due to their low interaction cross section with thermal neutrons.

Deposition of thin barrier films can be achieved through several processes including chemical vapor deposition (CVD) and physical vapor deposition (PVD). These processes can then be subdivided into more elaborate processes described by the process conditions such as plasma assisted CVD (PACVD), metallo-organic CVD (MOCVD), and method used in this work, metallo-organic fluidized bed CVD, (FB-CVD). Physical vapor deposition methods, being a "line-of-sight" deposition process, make obtaining uniform coatings on complicated geometries difficult [10-14, 17, 18]. PVD is not applicable to this work and will be not considered for this discussion.

Chemical vapor deposition is a process where one or more gases are mixed within a chamber that contains a substrate, and a reaction is then stimulated by a thermal, plasma, or radiation energy source. Nucleation and growth occur on the substrate surface, and the volatile byproducts of the reaction are transported from the chamber [13-15]. Since growth will occur on all available surfaces in the chamber, the chamber

can be modified to accommodate complex substrate geometries. For the purpose of coating particulate substrates, particles can be fluidized within the chamber, allowing the reactive gases to flow over and around the particles, evenly coating all available surfaces. This process of suspending a substrate within the reactive gas stream is known as fluidized bed chemical vapor deposition (FB-CVD).

The following sections describe the conception and development of a lab-scale FB-CVD system designed to create thin ZrN barrier coatings on U-7Mo particulate fuel. Section 2 will provide a brief literature review on chemical vapor deposition, precursor selection and fluidized bed technology. Section 3 describes the setup of each experiment system with detailed explanations of system components. Section 4 provides a summary of all experimental results with a brief description of how each experiment contributed to the evolution of each system design. Section 5 will present a discussion of the experiment results as well as the efficiency of the FB-CVD design for large scale applications. Finally Section 6 will present recommendations for system improvements to minimize contamination of future coating experiments utilizing the FB-CVD system.

The experiments were primarily completed using zirconia-silica microspheres as a surrogate for the U-7Mo particulate fuel. A major conclusion is the use of the solid tetrakis(dimethylamido)zirconium (TDMAZ) precursor is exceptionally challenging; significant process adjustments were required to utilize this precursor in the FB-CVD system. The final experiments performed produced coatings on fluidized microspheres heated to 275 ± 25°C at atmospheric pressure. The TDMAZ precursor was heated below the precursor melting point of 58°C without the use of ammonia in the deposition

process. The FB-CVD system is now operational, although a significant amount of work remains to optimize the chemical behavior of the system and reduce coating contaminants, nominal process variables have been defined and the deposition of thin zirconium-bearing barrier coatings has been demonstrated.

2. BACKGROUND

Fluidized bed chemical vapor deposition combines the deposition of a thin film in a reaction zone with the suspension of particles within a flowing gas. This section describes the relevant phenomena and systems parameters for FB-CVD technology with an emphasis on the deposition of zirconium nitride (ZrN). Section 2.1 reviews the fundamentals of chemical vapor deposition and Section 2.2 describes the precursor selection for ZrN. Section 2.3 describes fluidization technology for spouted fluidized beds.

2.1 Chemical Vapor Deposition

Chemical vapor deposition (CVD) is a process by which a thin, solid film is deposited onto a substrate surface through chemical reactions of a volatile molecular species in a gas phase [13-15]. The process relies on chemisorption process where the chemical interactions between the process gas and the substrate form strong ionic or covalent bonds. This is in contrast to physisorption where the molecule interacts with the surface through van der Waals forces [9]. The ionic nature of CVD makes it a "non-line-of-sight" process, where a film can be developed on complex structures with good step coverage and uniform thickness. The step-wise operation of the CVD process is represented in Fig. 1. First, one or more reactant gases, called precursors, are transported to a reaction vessel via an inert carrier gas stream. Within the reaction vessel, the substrate is heated to a predetermined temperature to induce the principle

chemical reaction either by thermal decomposition of a single precursor or by chemical interaction between multiple precursors. From the main gas flow, the reactants diffuse through the fluid boundary layer to the substrate surface where they are chemisorbed. The primary formation reaction occurs on the substrate surface and any by-products of the reaction are desorbed from the surface and carried from the reaction vessel by the carrier gas stream.

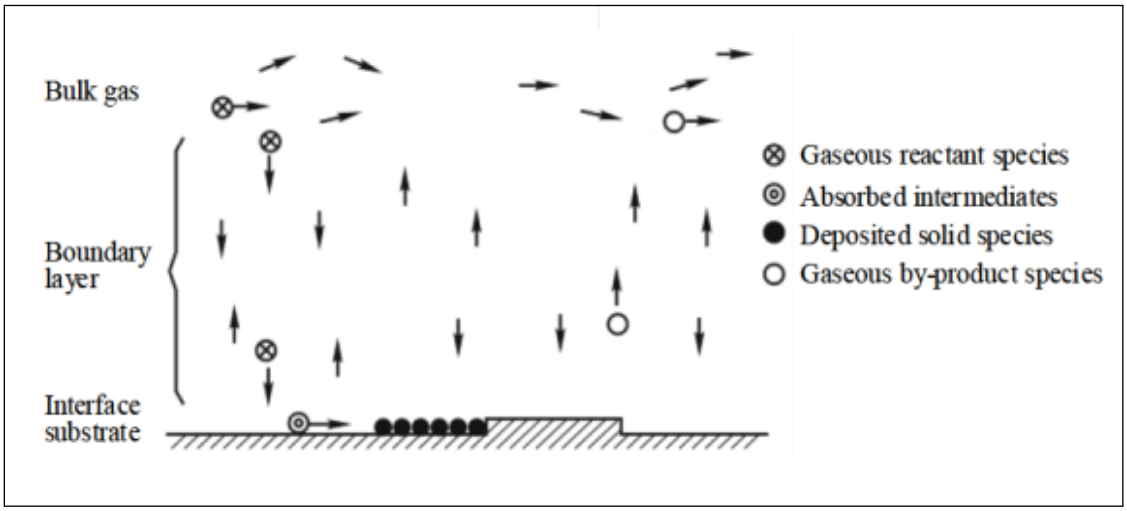

Fig. 1. Chemical vapor deposition process [11].

Early CVD processes required substrate temperatures greater than 900°C [14]. Higher temperatures can damage thermally sensitive substrates, requiring modifications to the typical CVD process to reduce the required temperature for reaction. Metallo-organic precursors are used to reduce the system temperature of the CVD process since their disassociation occurs at lower temperatures than inorganic precursors. Metallo-organic CVD (MOCVD) will be the focus of this research.

The literature concerning CVD systems is extensive, and the intermediate steps from generating a volatile gas, to the final film deposition must be refined for each new process. For brevity, this discussion will summarize the fundamental steps in the CVD process.

2.1.1 Fundamentals of Chemical Vapor Deposition

Deposition of a solid film from gas phase interactions can be understood from the equilibrium of a system: equilibrium is attained when the free energy of the system is minimized. With sufficient thermal energy, spontaneous reactions will occur to minimize the free energy of a system [13-15]. The change in Gibbs free-energy (ΔG) of the system provides a measure of the likelihood of a particular reaction and is a function of multiple parameters including the standard free energy of formation of each species considered, the absolute temperature of the system, and the partial pressure of each species [13].

System balance calculations are not always straightforward as there may be competing reaction pathways within a given CVD system. Metallo-organic molecules in particular can display complex dissociation patterns, substantially deviating from the theoretical products from a chemical balance equation. For example, the deposition of TiN using ammonia (NH_3) and tetrakis(dimethylamido)titanium (TDMAT) was examined in an experiment by L. Dubois utilizing infrared spectroscopy [16]. The desired reaction pathway is written as:

$$2Ti(NMe_2)_4 + 4NH_3 \rightarrow 2TiN + 4\,NMe_2 + N_2 + 2H_2$$
$$(Me=CH_3)$$

The experimental research found that multiple reaction intermediates are possible. An example is by the following reaction:

$$Ti_3\ (NMe_2)\ (NH_2)_2(N)_3 \rightarrow NH_3 + Ti_3\ N_4 + HNMe_2 2H_2$$

The product could reduce over the following pathways:

$$Ti_3\ N_4 \rightarrow TiN + 1/2N_2$$

$$Ti_3\ N_4 \rightarrow 3/2H_2 \rightarrow 3TiN + NH_3$$

Contamination within the system (oxygen, moisture, etc.) introduces additional possible chemical reactions with the precursor(s) present in the system. Therefore, experiments are performed under controlled conditions to optimize the process parameters to achieve the desired end product. Parameters of a system that can be optimized include the reactant transport to the substrate surface at a specified process pressure and the amount of energy used to initial the reaction.

Reactant Transport

Reactant transport occurs in two steps; transport to the reaction chamber followed by transport to the substrate surface. The process begins with generating a reactant species in gas phase. The gas is then transported to the reaction chamber via an inert carrier gas where it comes in contact with the heated substrate. Transport of the gas through the various pipes and valves of a system can be challenging since some reactant gases must be maintained at a higher temperature to remain in the vapor phase. Conversely, maintaining the transport conditions at too high a temperature can cause adverse reactions such as gas phase precipitation, where particles are homogeneously

nucleated in the gas phase. Gas phase precipitation can cause precipitant impurities in the deposit and also reduces the amount of reactants available at the substrate surface [10-15, 18].

Once the precursor gas enters the reaction chamber, they can be transported to the substrate surface. The transport of a gas molecule to the surface can be described by considering the fluid boundary layer. In 1904, Lewis Prandtl defined boundary layer theory, which combines ideas from theoretical hydrodynamics and experimental hydraulics to describe the viscous, shear, and inertial forces that occur near the surface of a solid that is moving through a liquid [19]. The boundary layer is the distance from the solid surface at which the velocity of the gas reaches 99% of the bulk gas velocity (Fig. 2).

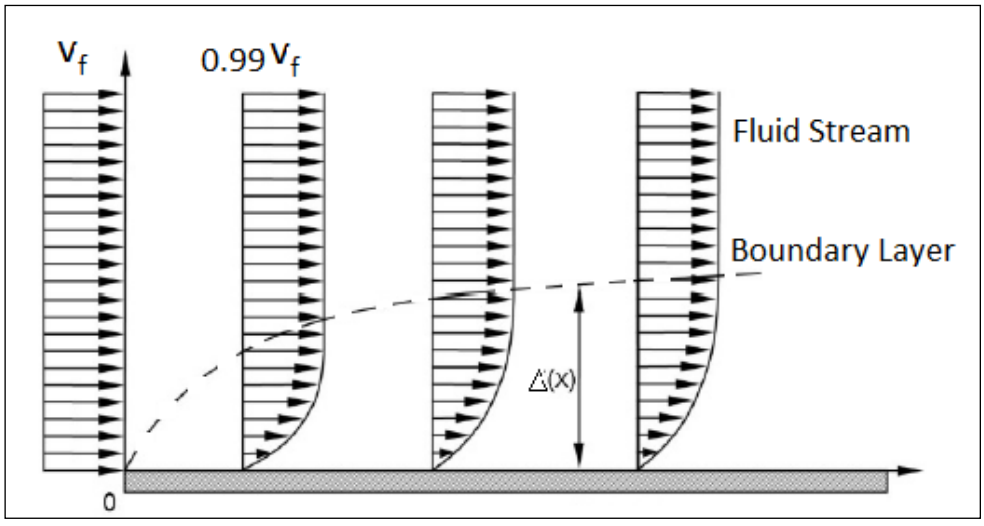

Fig.2. Boundary layer development over a flat plate [13].

The layer thickness (Δy) in Eq. 1, is characterized by the distance from the fluid inlet (x) and the Reynolds number for a particle ($R_{e,p}$). The Reynolds number in Eq. 2 is a dimensionless number that relates the inertial forces for a particle in terms of particle diameter (D_p), fluid density (ρ_f), and fluid velocity (v_f) to the viscous force in terms of fluid viscosity (μ_f).

$$\Delta y = \sqrt{(x/R_{ep})} \tag{1}$$

$$R_{ep} = (\rho_f \, v_f \, D_p)/\mu_f \tag{2}$$

From Eqs.1 and 2, a low pressure, low temperature system will have a thinner boundary layer than an atmospheric pressure, high temperature system. Diffusion of the reactants through the boundary layer and the diffusion of the by-products out of the layer is one of the main growth-rate limiting steps in the CVD reaction. A second growth rate control in the CVD system occurs when considering the concentration of reactants present within the process gas stream.

A system has that has a thin boundary layer will have a high diffusion coefficient which facilitates the transport of the reactants to the substrate surface. In such a system, the growth rate is controlled by the amount of reactants available. Conversely, a system with an excess amount of reactants available is rate controlled by the diffusion of the reactants through the boundary layer. A system can change from one rate-limiting step to the other through manipulation of process variables such as the substrate and gas temperatures, gas flow rates and system pressure.

Growth and Structure

The deposition rate and microstructure of the coating deposit can be controlled using temperature, pressure and saturation of the reactants [13-15]. Low temperature, low pressure systems typically produce fine grained structure deposits. High temperature, atmospheric systems will produce columnar deposits. The fine grained structure is desired for diffusion barrier coatings since a columnar structure will facilitate diffusion along the grain boundaries, although many coatings will be a combination of both structures [14]. However, the nominal low pressure required for fine grain generation is not as effective in a FB-CVD system due to the higher gas velocities needed for fluidization.

2.2 Metallo-Organic ZrN Precursors

The chemistry of CVD reactions is categorized by the potential reactions of the precursor(s). Metallo-organics deposit in a thermal decomposition reaction or pyrolysis where the precursor molecule splits into two or more elementary molecules [14-15]. The low binding energy in the metallo-organic molecules reduces the required substrate temperature to initiate the chemical reaction [11, 16, 17] and are therefore suitable for the coating process for the U(Mo) fuel particles. Metallo-organic precursors available for the ZrN MOCVD process include tetrakis(ethylmethylamino)zirconium (TEMAZ; $Zr[N(C_2H_5)(CH_3)]_4$), tetrakis(diethylamino)zirconium (TDEAZ; $Zr[N(C_2H_5)_2]_4$), and tetrakis(dimethylamino)zirconium (TDMAZ; $Zr[N(CH_3)_2]_4$). These precursors belong to the alkyls subset of metallo-organic precursors that include methyl and ethyl

hydrocarbons and start to decompose at 200°C [14]. The least hazardous and most cost effective precursor from this selection is the TDMAZ, which was used in the experiments described in Section 3 and 4.

Solid TDMAZ is a white/yellow crystalline material at room temperature with a melting point of 58°C [17, 27]. There is no documentation regarding the use of the TDMAZ precursor in the literature using atmospheric pressure CVD, (APCVD), and the vapor pressure and gravimetric analyses were not readily available [27]. However, research performed using plasma activated CVD indicated that deposited thin films were achieved using TDMAZ with substrate temperatures as low as 150°C and as high as 500°C and the subsequent films characterized were composed of zirconium, nitrogen, carbon and oxygen [17, 19, 30].

2.3 Chemical Vapor Deposition on Particulate Substrates

Coatings are deposited on all exposed surfaces of a heated substrate during the chemical vapor deposition process. Coating a particulate substrate requires that the process gas has sufficient contact with the entire surface of each particle [12]. A process gas can flow over and in between a packed bed of particles, but a uniform coating cannot be achieved due to particle-particle contact and particle contact with the reaction vessel walls. A solution is to create a bed of particles that are in constant motion relative to each other and the reaction vessel walls. Several methods, illustrated in Fig. 3 [20], are used in particle coating CVD systems to increase particle-gas contact by the movement

of particles [20]. The most commonly used method from Fig. 3 is the CVD of powders in a fluidized bed reactor [21].

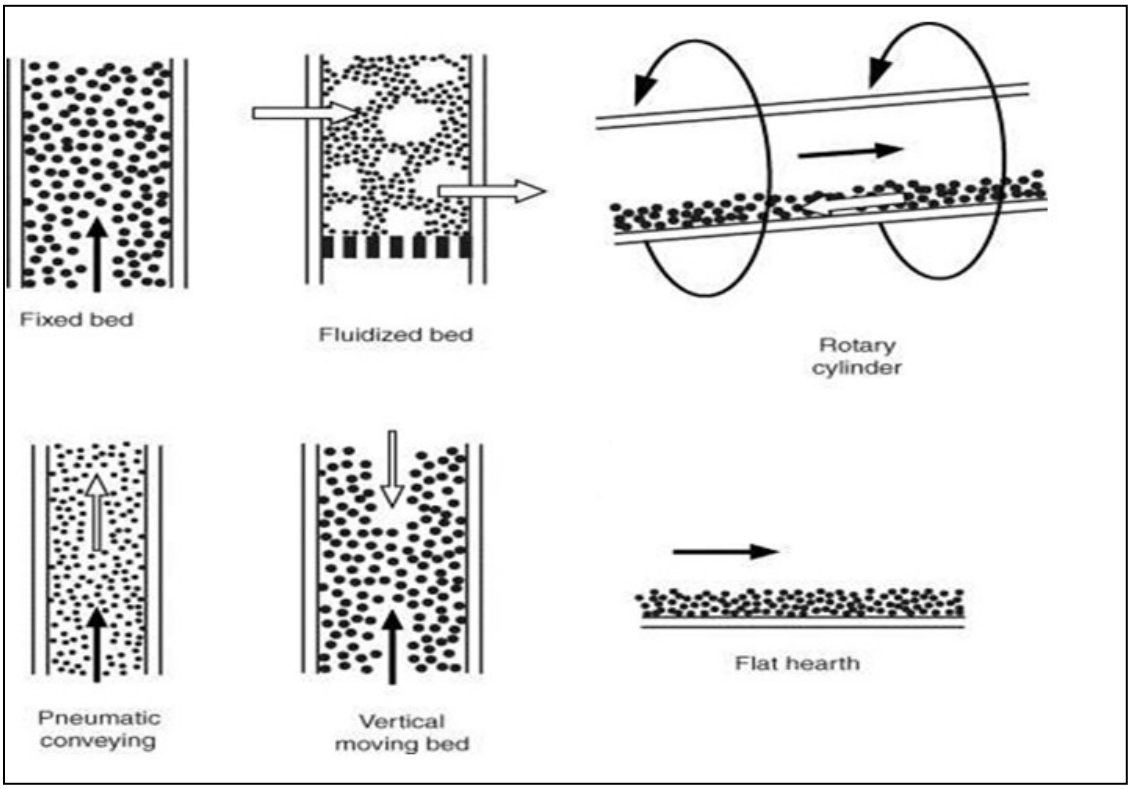

Fig. 3. Methods for increasing particle-gas contact in CVD.

2.3.1 Fluidized Bed

Fluidization is the process through which fine solid particles are made to behave like a liquid through contact with a gas. A bed of particles, initially at rest, comes in contact with an upward stream of gas. The fluidizing gas exerts an upward drag force as it moves around the particles, counteracting the force exerted by gravity. As the velocity

of the gas increases, the particles are put in motion. Increasing the flow rate further will suspend the particles within the gas stream creating a fluidized bed [12].

Fluidizing the substrate particles within the gas stream ensures efficient contact of the reactant gases with all available particle surfaces. This contact will result in high heat transfer between particles and a uniform heat distribution across the particle bed [20, 21]. Designing a fluidized bed requires knowledge about the size, shape and density of the particles to be fluidized. This information may then be used to calculate the minimum and maximum fluidization velocity to keep the particles suspended within the gas stream.

2.3.2 Fluidization Gas Flow Rates

The following discussion on fluidization is a brief synopsis from a very broad field; the section below is limited to the equations required for calculations to find the fluid velocity settings in the experiment system. Information on powder classification, particle-particle and particle-fluid interactions as well as bed pressure drop calculations and particle tortuosity may be found in references 20-23.

Fluidized beds are characterized by the fluidizing gas and the powder classification. To determine the fluidization mass flow rates for a specified system, the minimum fluidization velocity and as the terminal fluidization velocity may be calculated using the equations discussed below.

Incipient fluidization is the onset of fluidization for a particle bed and the minimum fluidization velocity is determined at this point. First the Archimedes number,

defined by Eq. 3 [21], is a dimensionless parameter that measures the ratio of the gravitational force in terms of gravity (g), particle density (ρ_p), particle diameter (d_p), fluid density (ρ_f) to the viscous force in terms of fluid viscosity (μ_f).

$$Ar = g d_p^3 \rho_f (\rho_p - \rho_f)/\mu_f^2 \tag{3}$$

The shape factor, φ, or sphericity of a particle, defines how close a particle is to a spherical shape. A particle's sphericity is defined in Eq. 4 [22] where the equivalent sphere is defined as a sphere with the same diameter as the particle being measured.

$$\varphi = (Surface\ \ area\ _{equivalent\ sphere})/(Surface\ area_{particle}) \tag{4}$$

The shape factor is difficult to measure directly since measuring the surface area of a particle can be challenging. The sphericity of some commonly fluidized particles is summarized in Table 1 [15].

Table 1. Sphericity of Commonly Fluidized Particles

Material	Sphericity
Sand	
Round sand	0.86
Sharp sand	0.66
Crushed sandstone	0.8–0.9
Coal	
Pulverized coal	0.73
Crushed coal	0.63–0.75
Activated carbon	0.70–0.90
Mica flakes	0.28
Fischer–Tropsch catalyst	0.58
Common salt	0.84
Crushed glass	0.65
Silica gels	0.70–0.90
Tungsten powder	0.89
Sillimanite	0.75
Wheat	0.85

Shape	Relative Proportions	Sphericity
Spheroid	1:1:2	0.93
	1:2:2	0.92
	1:1:4	0.78
	1:4:4	0.70
Ellipsoid	1:2:4	0.79
Cylinder	Height = diameter	0.87
	Height = 2 × diameter	0.83
	Height = 4 × diameter	0.73
	Height = $\frac{1}{2}$ × diameter	0.83
	Height = $\frac{1}{4}$ diameter	0.69
Rectangular parallelpiped	1:1:1	0.81
	1:1:2	0.77
	1:2:2	0.77
	1:1:4	0.68
	1:4:4	0.64
	1:2:4	0.68
Rectangular tetrahedron	—	0.67
Regular octahedron	—	0.83

A “round” shape has sphericity between $0.8 \leq \varphi \leq 1.0$, a “sharp” shape defined as $0.5 \leq \varphi \leq 0.8$, and particles with a sphericity of $0.1 \leq \varphi \leq 0.5$ are classified as “other” [22]. The following expressions in Eqs. 5-7 define the Reynolds number for minimum fluidization conditions from the Archimedes number (Ar) and Ergun’s equation for incipient fluidization for “round”, “sharp”, and “other” shapes respectively [22].

$$R_{e,mf} = \left(29.5^2 + 0.357Ar\right)^{1/2} - 29.5 \tag{5}$$

$$R_{e,mf} = \left(32.1^2 + 0.0571Ar\right)^{1/2} - 32.1 \tag{6}$$

$$R_{e,mf} = \left(25.2^2 + 0.0672Ar\right)^{1/2} - 25.2 \tag{7}$$

The minimum fluidization Reynolds number can be equated to the particle Reynolds number to find the minimum fluidization velocity for a particle of a specific shape, size and density.

Particle beds are usually composed of a range of particle sizes so the minimum fluidization velocity may be calculated for the largest size range in the particle distribution. The fluid velocity should be enough to fluidize the largest particles but not high enough to entrain smaller particles in the gas stream out of the reaction chamber. The terminal velocity is calculated as an upper bound for the fluid velocity in Eq. 8 [23].

$$v_T = [2g(D_p)^2(\rho_p - \rho_f)]/18\mu \tag{8}$$

where D_p is the diameter of the particle, g is gravity g, ρ_p is the particle density, ρ_f is the fluid density and μ_f is the fluid viscosity.

3. EXPERIMENT DESIGN AND PROCEDURE

The FB-CVD experiment used argon gas (99.99%) purchased from BOTCO AOC (Bryan, TX), electronic grade ammonia gas (99.9992%) from Matheson (Houston, TX), and TDMAZ crystals (>99.99%) purchased from STREM Chemicals Incorporated (Newburyport, MA). The coating experiments were performed on the following substrates: 1 mm O.D. tungsten or molybdenum wires, ZrO_2-SiO_2 microspheres (185 to 250 μm), and tungsten powder (75 to 250 μm) available in the Fuel Cycle and Materials Laboratory (Texas A&M) and un-enriched U-7Mo microspheres (45 to 125 μm) obtained from Idaho National Laboratory (Idaho Falls, ID). Gas flow rates and substrate temperature were used as the principle process variables. The reaction vessel and precursor delivery vessel were loaded and unloaded inside of an inert argon atmosphere glovebox to minimize contamination with oxygen and moisture in the air.

The experimental system design evolved as the experiments progressed. A spouted fluidized bed design was used initially and an inverted fluidized bed was used in the final experiments. Section 3.1 and 3.2 will describe the components of the spouted and inverted fluidized bed systems, respectively, as well as the experimental procedure developed for each system. Section 3.3 reviews the methods used to prepare samples from each experiment for characterization and the tools used for the process. Results from the experiments performed with each system are provided in Section 4.

3.1 Spouted Fluidized Bed Reactor

3.1.1 System Components

A schematic of the main components in the spouted FB-CVD system is provided in Fig. 4.

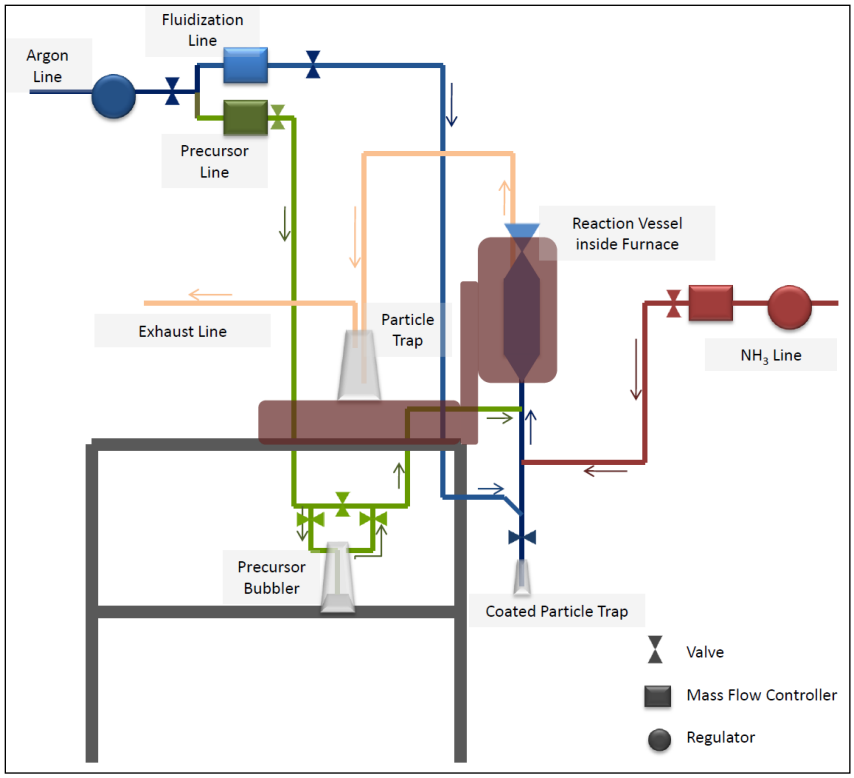

Fig. 4. Schematic of the spouted FB-CVD system.

All gas lines in this system were made using 0.6 cm (1/4 in) diameter stainless steel tubing. The connections between the components and the tubing were formed using stainless steel Swagelok fittings. The valves were stainless steel Swagelok quarter-turn plug valves and Swagelok needle valves unless otherwise noted.

Connections between the stainless steel tubing and the glass components of the system was achieved using ~1 cm (3/8 in) diameter Swagelok Ultra-Torr vacuum fittings with high temperature Viton O-rings. Type K thermocouples (Omega KQXL-116G-12) connected to a temperature data logger (Omega OM-CP-OCTTEMP2000-CERT) were used to monitor the temperatures of the system components.

The argon supply line (upper left of Fig. 4) was divided between two mass flow controllers: a high-flow mass flow controller (Omega model FMA5524) to provide the fluidization gas and a low-flow mass flow controller (Omega model FMA5508) to provide the carrier gas for the TDMAZ precursor. The high-flow line entered the reactor from the bottom inlet. The low-flow argon line is passed through the heated precursor bubbler to carry the precursor vapor to the inlet line for the reaction vessel. The ammonia (NH_3) tank was connected to a low-flow mass flow controller (Omega model FMA5508ST) and that supply line enters the flow path to mix with the precursor and high-flow argon gases prior to entering the reaction vessel. The hot wall reaction vessel was placed in a vertical tube furnace (Barnstead Model F21135) for heating the particulate substrate during fluidization. The off-gas exits the reaction vessel from the top; over-fluidized particles and solid by-products are collected in a particle trap prior to gas scrubbing and exhaust through a fume hood. The entire system was assembled inside of a fume hood due to the hazardous nature of the TDMAZ and ammonia.

The precursor bubbler was heated using a heater cartridge (McMaster-Carr model 3540K32) submerged in a silicon oil bath. The lines leading from the bubbler to the reaction vessel were wrapped with silicon heater tape (OMEGA model SRT051-

120LSE) to prevent precursor condensation during transport. Two variable autotransformers (Staco Energy model 3PN1010B) were used to adjust the temperature of the heater tape and the heater cartridge.

All glassware used in this system was created at the Texas A&M University (TAMU) chemistry glass shop. All modifications and repairs to glassware in the system were also completed at the TAMU glass shop. Details of the design and use of each system component are provided below.

Reaction Vessel

The reaction vessel design was based on a style known as a spouted bed reactor [21]. The original reaction vessel, as depicted in Fig. 5, was crafted from quartz glass with a maximum outer diameter of ~5.08 cm (2 in) and an inlet and outlet outer diameter of 0.635 cm (1/4 in). The furnace utilized in the experiment was the limiting factor in determining the design of the vessel height and diameter.

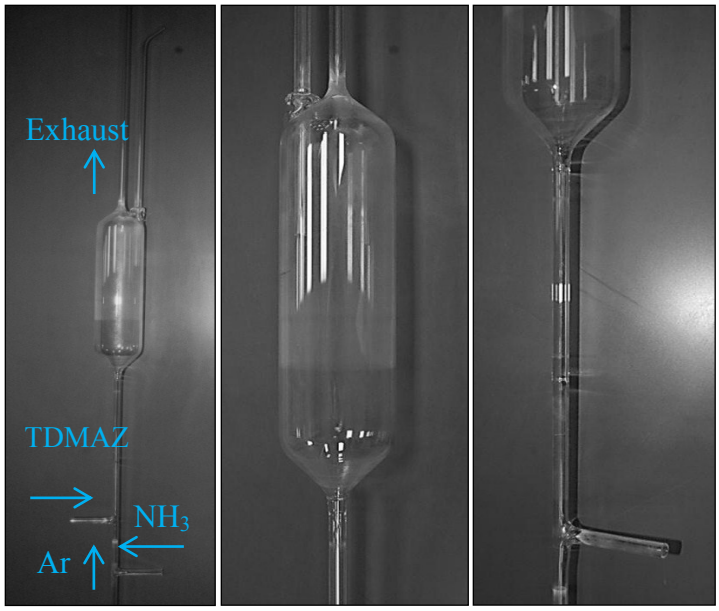

Fig. 5. Quartz spouted fluidized bed reactor.

The high-flow argon fluidization gas entered through the inlet at the bottom of the primary center tube. The secondary lines for the ammonia and the vaporized TDMAZ precursor (carried by the low-flow argon) entered the stream just below the spouted bed from the right and left of the primary tube respectively. The top center exit line was used for powder insertion and the parallel line on the right was the exhaust line leading to the particle trap and exhaust gas scrubber.

This initial design was used to validate the fluidization calculations for the diameter and height of the fluidized bed with different particulate sizes, shapes, and densities. This setup was also used for the wire coating experiments. However, the design required modifications to enable easier and safer loading of particulate substrates.

The reactor was changed to a Pyrex based design with the same vessel dimensions; the components are shown below in Fig. 6.

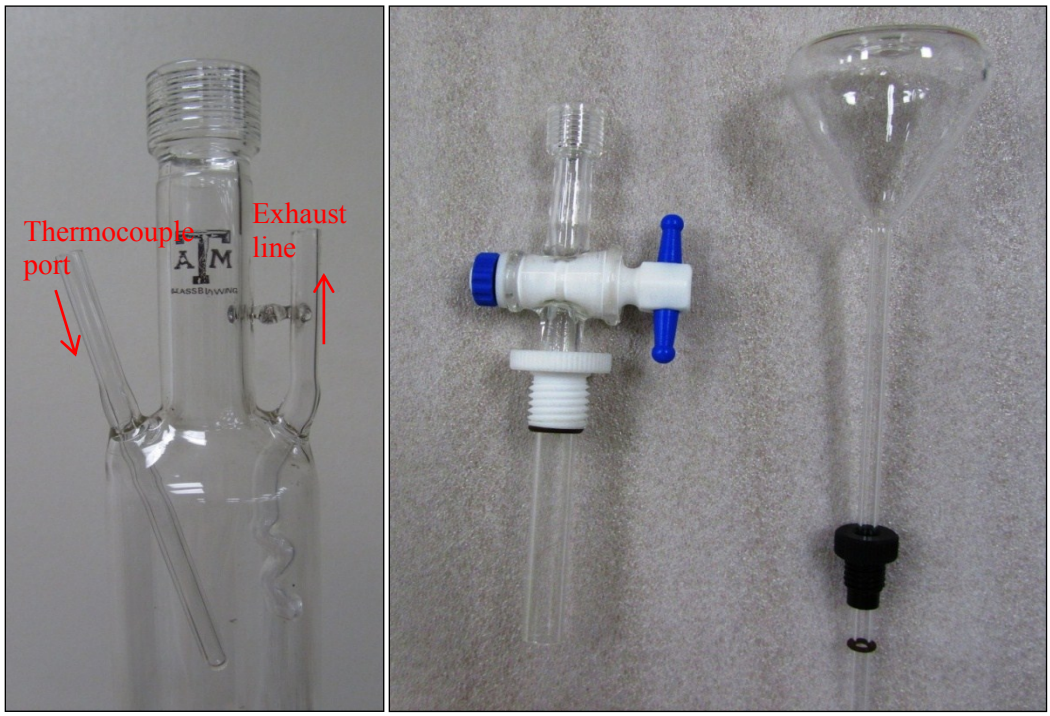

Fig. 6. Top loading components of the Pyrex spouted fluidized bed reactor [main reaction vessel (left), glass assembly with Teflon valve (center), and powder substrate vessel (right)].

The main reaction vessel, shown on the left of Fig. 6, remains connected to the system assembly throughout the experiment. The main reactor vessel included three attachment points. The glass outlet line on the right of the vessel was the exhaust gas line leading to the particle trap and exhaust gas scrubber. The glass tube on the left holds the thermocouple during system operation. The top center opening of the vessel held the substrate loading container.

The vessel component on the far right of Fig. 6 is the container used to hold the particulate substrate. This container was filled in an inert atmosphere glovebox and secured into the glass assembly with the black Teflon plug and Viton O-ring (Fig. 6 center). The Teflon valve was closed while transporting the loaded container from the glovebox to the vessel during the system assembly. The glass assembly was screwed into the top of the reaction vessel with the white Teflon plug and Viton O-ring. At the conclusion of the heat and purge cycle, the valve on the glass assembly was rotated open and the substrate holder was inserted through the hole in the valve to release the powder into the reaction vessel. The assembled vessel is shown in Fig. 7.

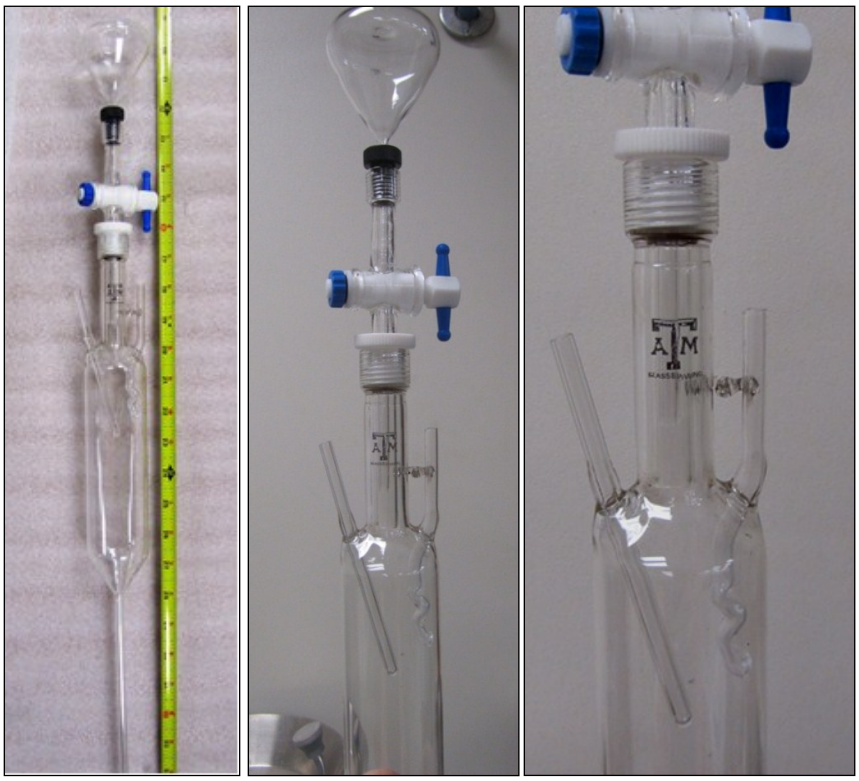

Fig. 7. Assembled spouted Pyrex fluidized bed reactor.

Coated Particle Trap

The coated particle trap (Fig. 8) was created to collect the coated particles at the conclusion of each experiment.

Fig. 8. Coated particle trap.

The trap was made from Pyrex glass with Teflon valves. The top "Y" shaped section serves as the inlet for the high-flow fluidization gas on the right and the tube on the top connects to the bottom of the reaction vessel with an ultra-torr glass to glass vacuum fitting. When the fluidization gas flow is terminated, the particles fall from the reaction vessel into the coated particle trap. The top "Y" section may be removed from the hole in the Teflon valve so that the valve may be rotated, isolating the particles from

the outside environment. The "Y" tube must be fully withdrawn from the vessel so the vessel can be completely removed from the system. The coated particle trap may then transported and stored with the coated particles in the glovebox at the conclusion of each experiment.

Precursor Bubbler I

The bubbler used to vaporize the TDMAZ crystals (Fig. 9) was created from Pyrex glass and Teflon valves. The TDMAZ crystals are air and moisture sensitive so the bubbler was designed to be loaded in the glovebox and sealed for transport and inclusion into the system assembly. The precursor crystals are loaded from the top and the glass lid is secured with a clam clamp and a Viton O-ring.

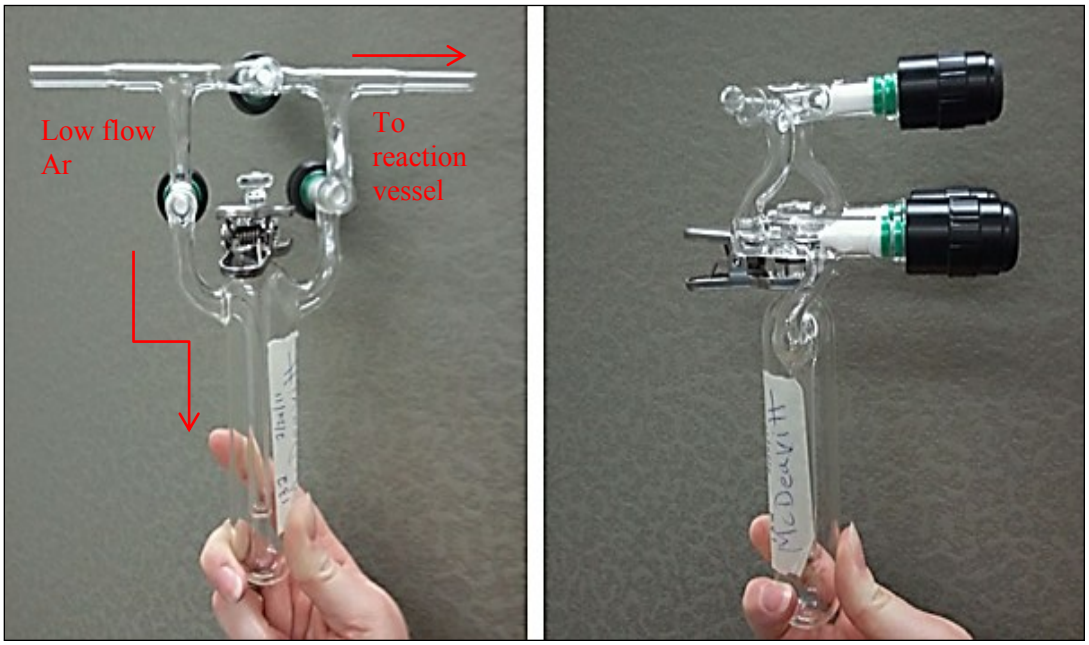

Fig. 9. Precursor bubbler I: Pyrex bubbler.

During the purge phase, the bottom left and right valves are shut and the top valve opened to bypass the precursor crystals while purging and heating the system. After the system purge, the valve on the top is closed and the bottom valves opened to allow the carrier gas to enter the bubbler via the inlet (left) and pass over the heated crystals, carrying the vaporized precursor from the bubbler via the outlet on the right.

The bubbler in Fig. 9 had several issues pertaining loading and unloading of the precursor crystals. The precursor was also never completely consumed during each experiment so a new bubbler was created.

Precursor Bubbler II

The second bubbler design (Fig. 10) was created from Pyrex glass and has a fritted glass plate in the center of the vessel. The white Teflon plug may be removed from the top for precursor crystals insertion onto the fritted plate. The vessel is sealed with a Viton O-ring connected to a Teflon plug that screws into the top. The carrier gas enters through the left inlet tube and flows upward through the fritted plate from below. The gas flows around and through the crystals fluidizing them to ensure maximum contact. The saturated carrier gas then exits through the outlet on the right. The valves on this system may be rotated shut to isolate the precursor from air while transporting the bubbler from the glovebox to the system assembly and during the system purge.

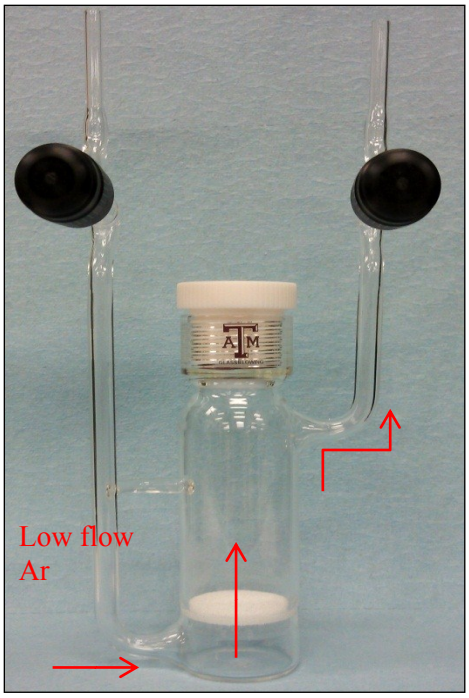

Fig. 10. Precursor bubbler II: fritted Pyrex bubbler.

3.1.2 Experiment Procedure

Experiments completed with the spouted fluidized bed reactors described above followed the procedure outlined below; specific temperatures and flow rates varied and will be discussed in Section 4 for each individual experiment.

1. The system was heated and purged with argon gas for 3 hours prior to each experimental run.
2. The bubbler was loaded with TDMAZ crystals in the inert atmosphere glovebox, sealed, and transferred to the system assembly where it was heated to a predetermined temperature.

3. The high flow argon controller was set at the fluidization flow rate and the particulate substrate released into the reaction vessel.
4. The precursor bubbler bypass valve was closed and the bubbler and the ammonia line valve were opened to the reaction vessel.
5. At the conclusion of the experiment, the ammonia and bubbler valves were shut while the argon continued to flow through the vessel, purging any remaining precursor vapor from the system.
6. The furnace, heater tape, and heater cartridge were shut down.
7. The argon valve was closed and the coated particles dropped into the particle trap. The particle trap was then sealed, removed from the system, and transferred to the glovebox.

3.2 Inverted Fluidized Bed Reactor

3.2.1 System Components

System II was designed as an inverted fluidized bed reactor. A schematic of the main components in each FB-CVD setup is provided in Fig. 11.

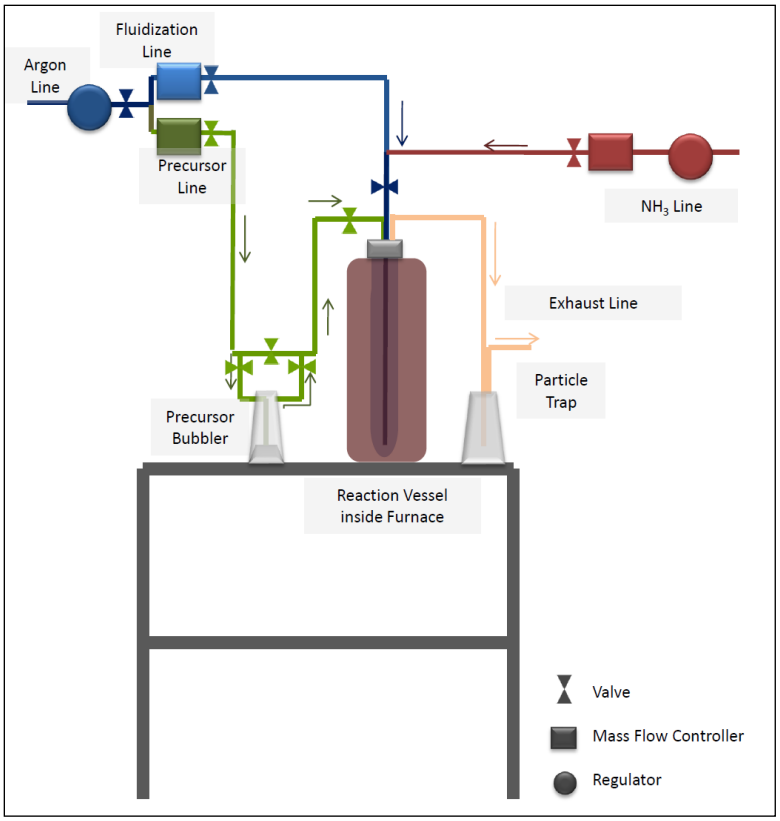

Fig. 11. Schematic of the inverted FB-CVD system.

The design of the inverted FB-CVD system incorporated many of the spouted bed system components described in Section 3.1. The 0.635 cm (1/4 in) stainless steel gas lines connecting directly to system components were replaced with 0.635 cm (1/4 in) PTFE tubing. The valves are Swagelok quarter turn plug valves and needle valves unless otherwise noted.

The reaction vessel was placed inside a moveable aluminum metal annulus that was heated externally with high temperature fiberglass heater tape (Omega model DHT051040LD). The temperature of the heater tape was controlled with a variable autotransformer (Staco Energy model 3PN1010B).

Reaction Vessel II

Reaction vessel II is an inverted fluidized bed schematically pictured in Fig. 12. The top half of the vessel is made from an aluminum section welded to a Swagelok Ultra-Torr vacuum fitting and the stainless steel gas inlet/outlet lines. A 2.54 cm (1 in) outer diameter Pyrex glass tube serves dually as the reaction vessel and particle containment vessel and is secured to the aluminum housing with a 2.54 cm (1 in) Swagelok Ultra-Torr vacuum fitting and a high temperature silicon O-ring. All gas lines leading to and from the vessel were sealed with the Swagelok valves. A rotary vane pump was attached to the end of the exhaust system to facilitate fluidization with the new vessel. The vessel can be loaded within the glovebox by unscrewing the Ultra-Torr fitting that clamps the O-ring to the glass tube. The glass tube then slides out of the aluminum housing for loading/unloading or cleaning purposes.

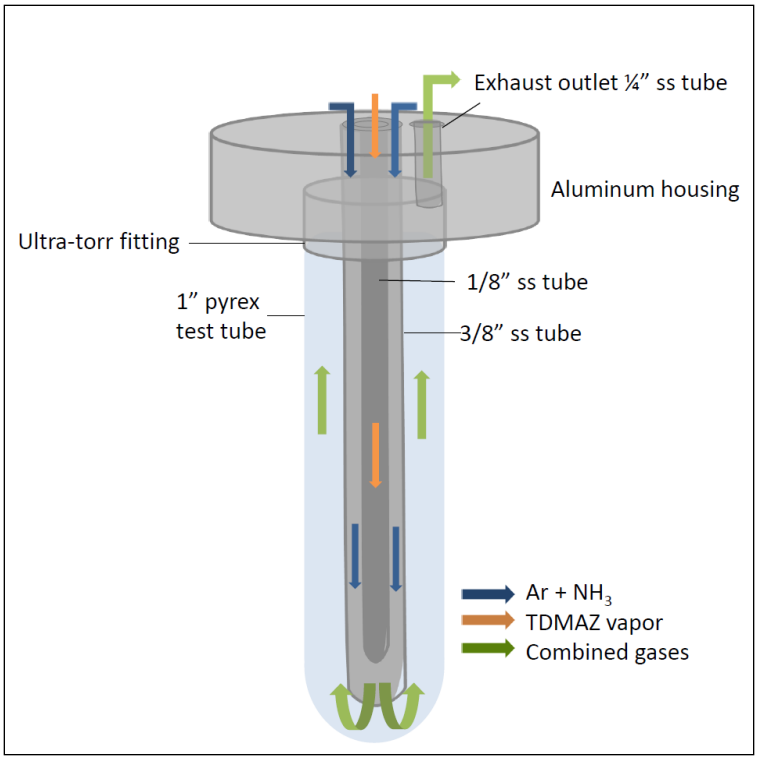

Fig. 12. Schematic of the inverted fluidized bed reactor.

The gas inlet consists of two tubes, a 0.952 cm (3/8 in) outer diameter stainless steel tube and a second 0.317 cm (1/8 in) outer diameter stainless steel tube placed inside the first. The first tube carries the ammonia and fluidization argon gas and the second carries the precursor vapor. The two gas streams are separate until they enter at the bottom of the vessel in the hot zone of the system. The gas flow is reversed at the bottom of the tube and the redirected flow fluidizes the particles around the stainless steel lines. The exhaust gas exits through the 0.635 cm (1/4 in) stainless steel tube on the top of the reaction vessel.

Precursor Bubbler III

The third precursor bubbler (Fig. 13) was a Swagelok stainless steel sample cylinder coupled with 0.317 cm (1/8 in) stainless steel tubing and Swagelok valves and fittings. The stainless steel is corrosion resistant to the TDMAZ crystals and the vessel design is easier to seal, assemble, and clean. This bubbler was heated using heater tape and placed within 30.5 cm (12 in) of the reaction vessel, reducing the distance the precursor had to travel in the vapor phase.

Fig. 13. Precursor bubbler III: stainless steel bubbler.

The argon carrier gas flows from the top valve through the 0.317 cm (1/8 in) stainless steel gas tube. The tube extends to the bottom of the steel cylinder where the

carrier gas flows over the precursor crystals. The saturated vapor flows around the 0.317 cm (1/8 in) tube and exits to the reaction vessel through the 0.635 cm (1/4 in) tube on the right. The bubbler may be sealed using the Swagelok valves on either end.

3.2.2 Inverted Bed Experiment Procedure

Experiments run with the inverted fluidized bed reactor followed the procedure outlined below; specific temperatures and flow rates varied and will be discussed in Section 4 for each individual experiment.

1. The system was heated and purged with argon gas for 3 hours prior to each experimental run.
2. The particulate substrate was loaded into the reaction vessel in the glovebox, sealed, and then transferred to the system assembly.
3. The bubbler was loaded with TDMAZ crystals in the inert atmosphere glovebox, sealed, and transferred to the system assembly where it was heated to a predetermined temperature.
4. The precursor bubbler bypass valve was closed and the bubbler and the ammonia line valve were opened to the reaction vessel.
5. At the conclusion of the experiment, the ammonia and bubbler valves were closed and the heater tape and heater cartridge were shut down, while the argon continued to flow through the vessel, purging any remaining precursor vapor from the system.

6. The valves on the top of the vessel were closed, sealing the coated particles inside. The vessel was removed from the system and transferred to the glovebox.

3.3 Sample Preparation and Characterization

Samples were prepared and taken to the electron microprobe laboratory located at the Texas A&M Geology department. Samples were examined and characterized with wavelength dispersive spectroscopy (WDS), energy dispersive spectroscopy (EDS) and backscatter electron imaging (BSE) using a four-spectrometer Electron Probe Micro-Analyzer (EPMA: Cameca model SX50) equipped with a PGT energy dispersive system and a dedicated Sun workstation used for image analysis [24].

3.3.1 Sample Preparation

Samples collected from each experiment were photographed using a Hirox microscope. The samples were then ultrasonically cleaned in ethanol and set in epoxy resin for polishing. Next, the samples were sanded by hand using 600-grit silicon carbide (SiC) paper to reach a clean cross section of the material. Hand polishing of the samples continued, using progressively smaller grit size down to 1200-grit SiC paper. Final polish of the samples was achieved using 1/4 μm diamond suspension on nylon paper with an automatic Mini-met polisher. Polished samples were ultrasonically cleaned with ethanol and then carbon coated before placement in the EPMA.

4. RESULTS

The results described in this chapter comprise the pre-experiment design calculations and measurements (Section 4.1) and a description of twelve FB-CVD experiments (Sections 4.2 to 4.4) leading to the formation of thin zirconium-bearing coatings. Table 2 outlines the outcomes from these activities with cross references to the Sections describing the experimental system configurations from Section three.

Table 2. Outline of Calculation and Experimental FB-CVD Results

Experiment Section	System Description Section	Description	Substrate	Coating Observed? (Y/N)
4.1	N/A	Particle fluidization calculations and test	Zirconia-silica microspheres and tungsten particles	N/A
4.2	3.1	Quartz spouted fluidized bed	Molybdenum wire and tungsten particles	Yes
4.3	3.1	Pyrex spouted fluidized bed	Molybdenum wire and U(Mo) microspheres	No
4.4	3.2	Inverted fluidized bed	Zirconia-silica microspheres and tungsten wire	Yes

4.1 Determination of Fluidization Parameters

4.1.1 Fluidization Calculations

The equations described in Section 2.3.2 were used to estimate the minimum gas velocity to induce fluidization for three types of powder materials. In addition to the calculations, fluidization tests were performed at a room temperature of 23ºC (see Section 4.1.2). The calculations and measurements were made for zirconia-silica microspheres (185 to 210 μm), U-7Mo microspheres (45 to 125 μm), and tungsten powder (60 to 250 μm). The relevant physical data for the powders is provided in Table 3.

Table 3. Physical Data for the Particle Substrates

	Density (g/cc)	**Size Range-x (μm)**	**Shape factor**
Zirconia-Silica	4.56	210 < x < 185	round
U-7Mo	14.3	125 < x < 45	round
Tungsten	19.25	250 < x < 60	sharp

The basic thermophysical properties for the argon fluidizing gas were obtained from NIST Chemistry WebBook [27]. The viscosity of a gas increases with increased temperature since the higher kinetic energy of the gas molecules increases the probability of molecule-molecule collision, increasing the resistance to flow. The density decreases with increasing temperature as shown for argon in Fig. 14. The minimum fluidization velocity calculations are dependent on the density and viscosity of

the fluidizing gas. Since the measurements were made at room temperature the fluidization conditions were expected to change for actual FB-CVD conditions at 200°C to 400°C. The Archimedes number from Eq. 3 is directly proportional to the fluid density and inversely proportional to the viscosity of the fluid. The increased viscosity will therefore have the effect of lowering the minimum fluidization of a particle of size d_p and particle density, ρ_p.

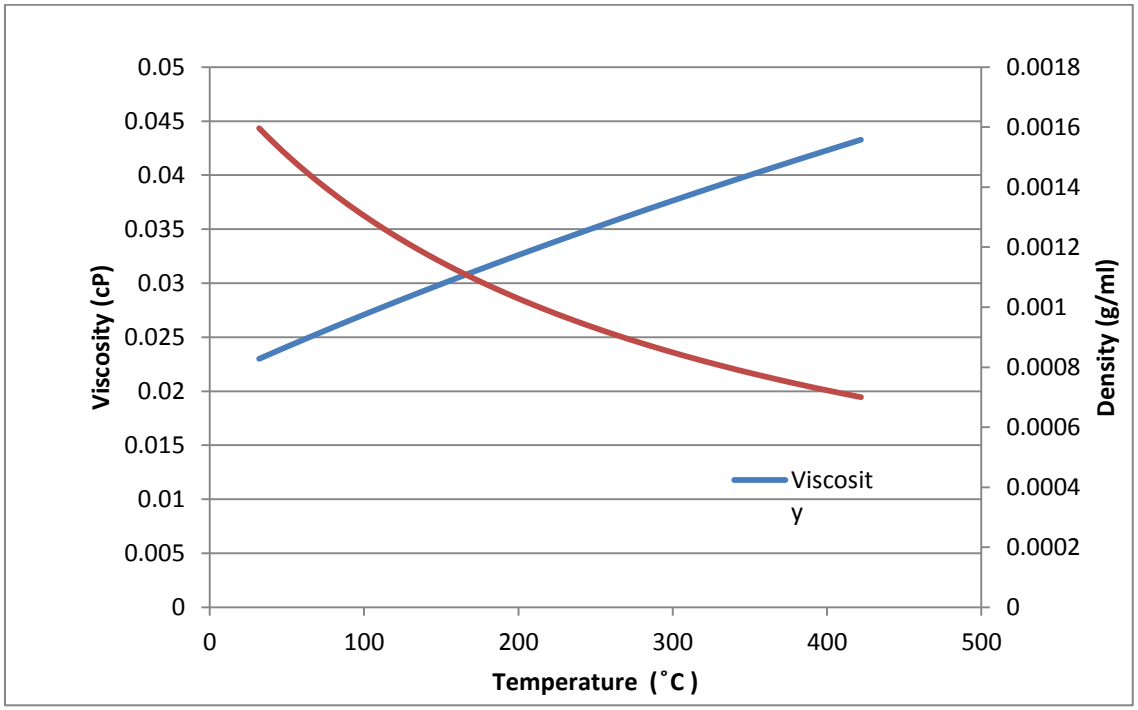

Fig. 14 Thermophysical properties of pure argon gas at 1 atm and varied temperature.

Figure 15 is a picture of the zirconia-silica microspheres (right) and the tungsten particles (left), the U-7Mo particles were not available for the initial fluidization tests. The microspheres were classified as "round" and the tungsten particles classified as

"sharp" by referencing Table 1 from Section 2. Equations 5 and 6 were used to calculate the minimum fluidization velocity for the upper diameter size for each type of powder.

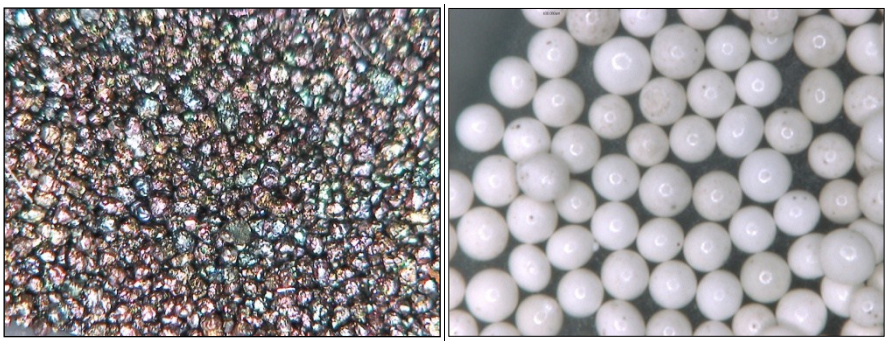

Fig 15. Images of the particle substrates tungsten particles (left) and the zirconia-silica microspheres (right).

Table 4 provides representative results for the fluidization calculations of the 210 μm, U-7Mo microspheres, at varied system temperatures. Fig.16 is a plot of the three types of particulate substrates with a 210 μm diameter, over the various operating temperatures and Fig. 17 is a plot of the calculated mass flow rates for the U-7Mo microspheres, of varied sizes, over the range of predicted operating temperatures.

Table 4. Calculated Minimum Fluidization Flow Rate for U-7Mo Microspheres

	Temperature (°C)					
	23	**150**	**200**	**250**	**300**	**400**
Ar	4.25E-05	1.74E-05	1.31E-05	1.01E-05	8.03E-06	5.39E-06
Re, mf	2.57E-09	1.05E-09	7.9E-10	6.11E-10	4.86E-10	3.26E-10
Velocity (cm/s)	1.67E-04	1.26E-04	1.16E-04	1.07E-04	1.00E-04	8.92E-05
Mass Flow (L/min)	3.17	2.41	2.21	2.04	1.91	1.69

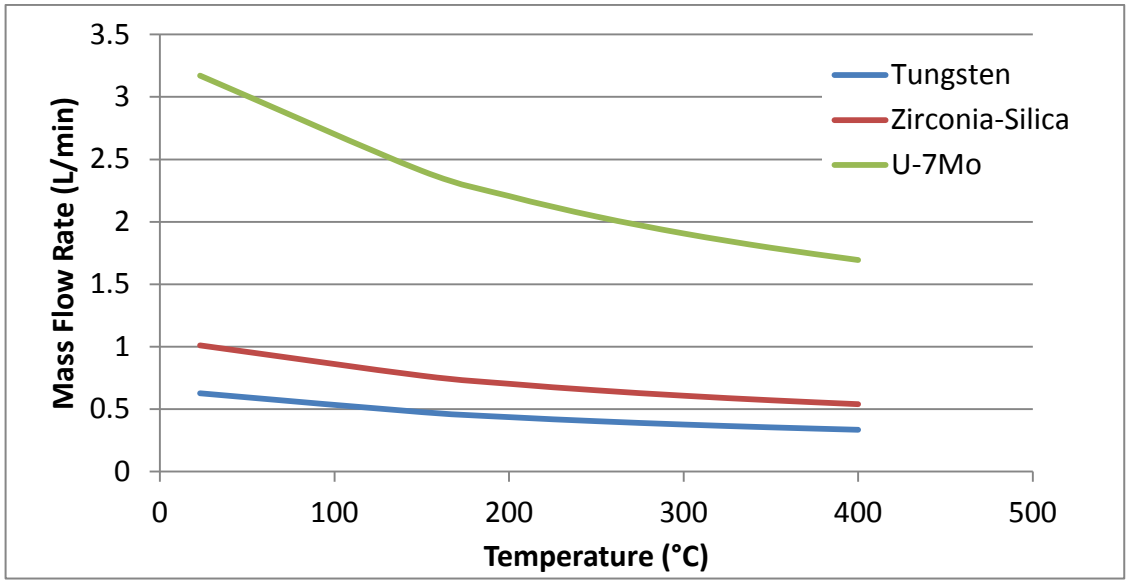

Fig. 16. Comparison of the minimum fluidization mass flow rates vs. temperture for the tungsten, zirconia-silica and U-7Mo powders.

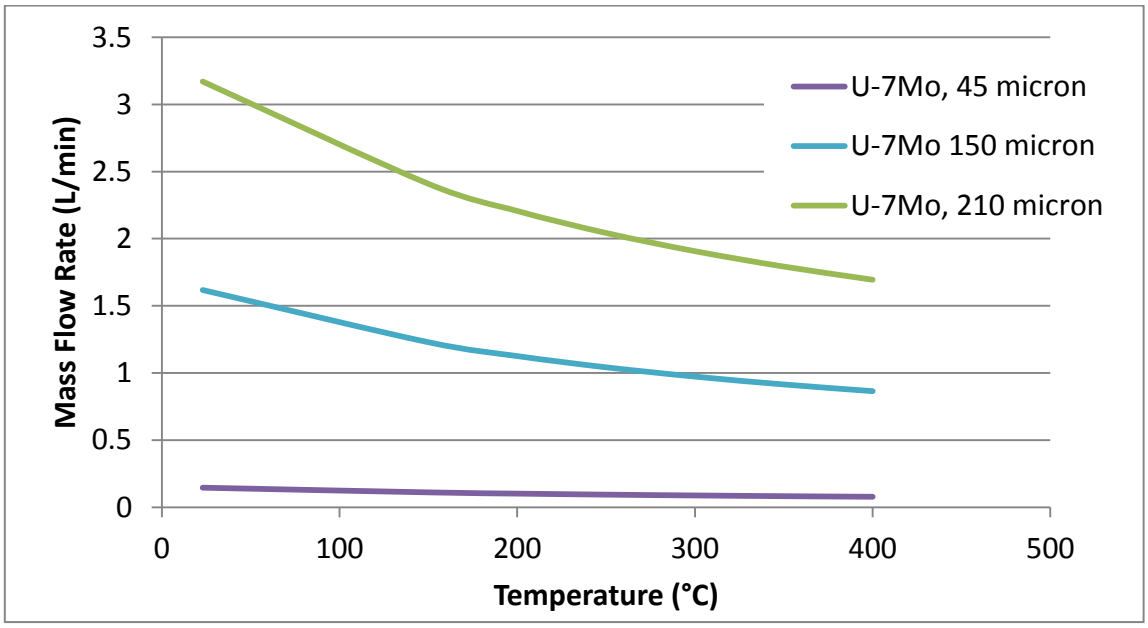

Fig. 17. Comparison of the minimum fluidization mass flow rates vs. temperature for large large (210 µm), medium (150 µm), and small (45 µm) U-7Mo microspheres.

The U-7Mo particles will require the highest mass flow rate to remain fluidized. The mass flow rate required to maintain a fluidized state changes over the operating temperature of the system, so it was determined that the system should have already achieved a steady state temperature before inserting the particles into the reation vessel. Another observation from Fig. 16, is that the particles deviation from a spherical shape require a lower mass flow rate than the round particles. To illustrate this further, Fig. 18 is a plot of the zirconia-silica predicted fluidization condition calculated for "round" and "sharp" particles. This introduces a new challenge as not all particles classified as "round" are expected to be perfect spheres due to manufacturing defects. The plots of the predicted mass flow rates show that any particles classified as "sharp" will over fluidize out of the reactor.

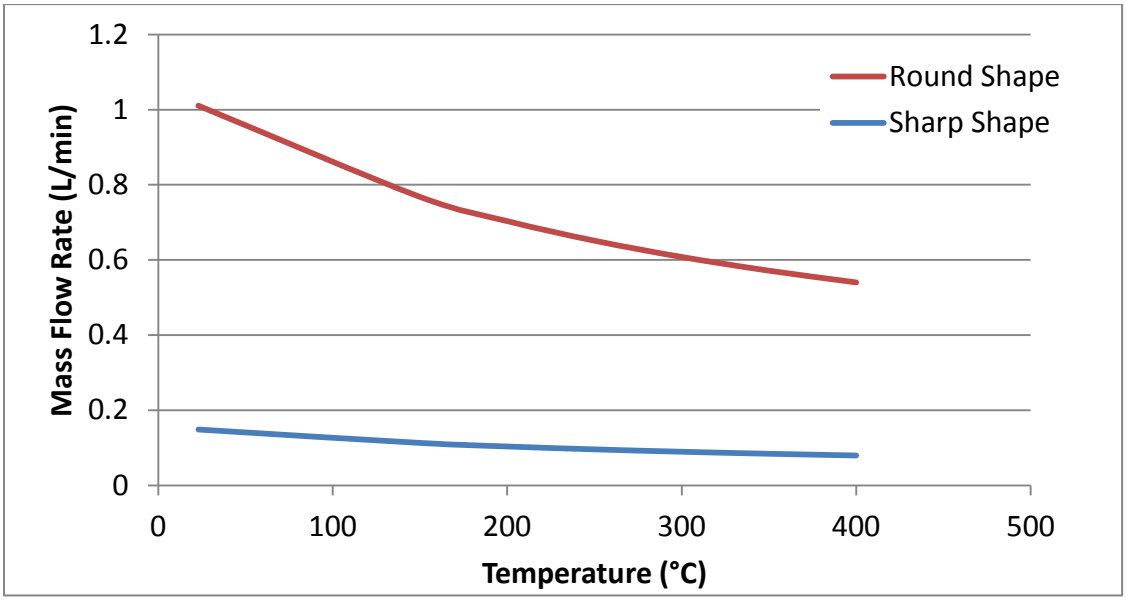

Fig 18. Comparison of the minimum fluidization mass flow rates vs. temperature for zirconia-silica particles, "round" vs "sharp" shape.

4.1.2 Fluidization Tests

Minimum fluidization flow rate measurements were performed at 23°C and 1 atm conditions. The fluidization test proceeded on the benchtop with the zirconia-silica microspheres and tungsten particles, shown in Figs. 19 and 20 respectively. The zirconia-silica microspheres fluidized at a mass flow rate of 1.3 L/min compared to a calculated value of 1.01 L/min. The tungsten particles fluidized at a flow rate of 4.7 L/min compared to a calculated value of 4.26 L/min.

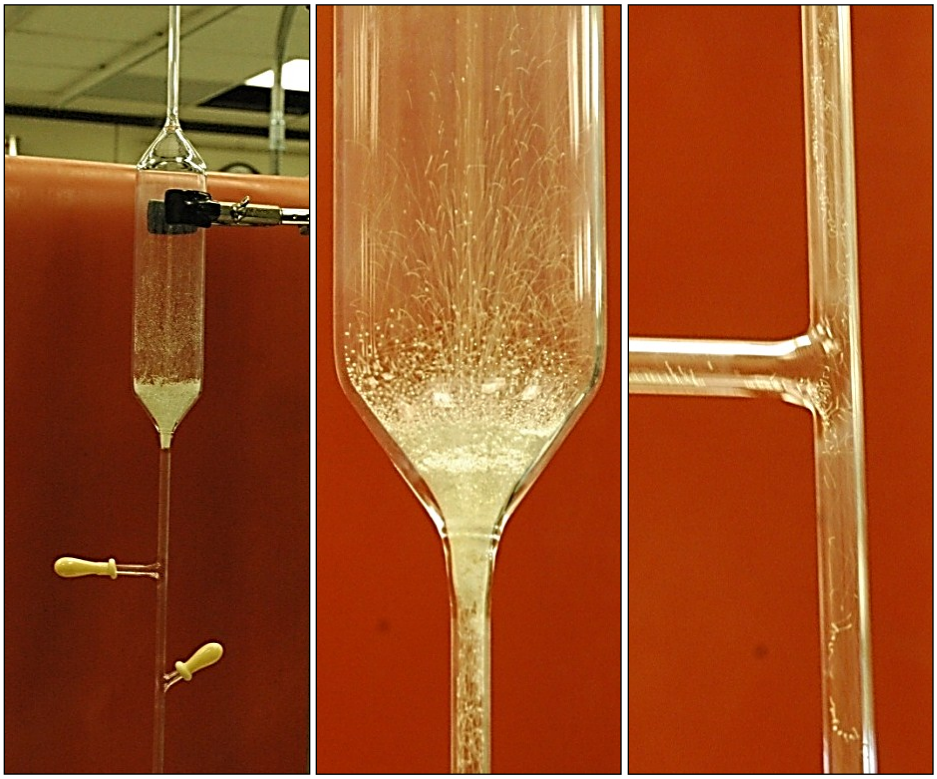

Fig. 19. Minimum fluidization flow rate measurements of the zirconia-silica microspheres.

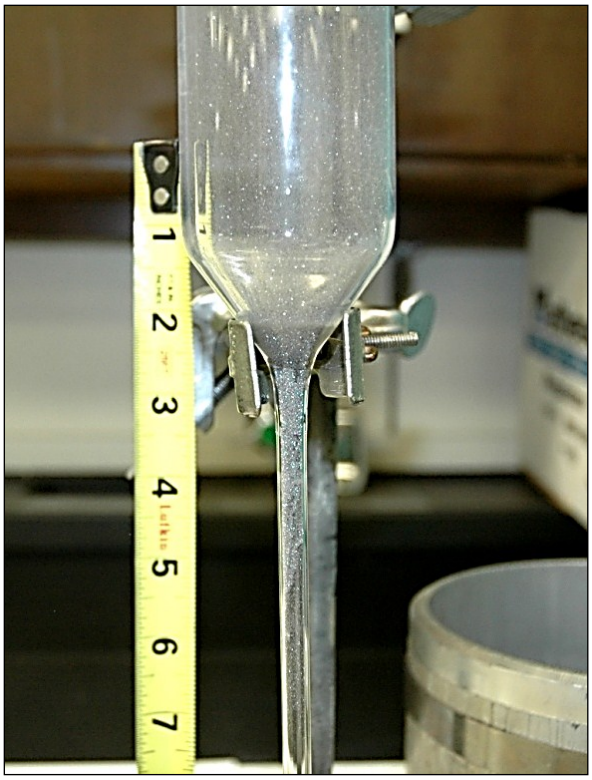

Fig. 20. Minimum fluidization flow rate measurements of the tungsten particles.

Observed in both fluidization tests, the particles fluidized lower in the reaction vessel than expected. The left of Fig. 19 shows the particles entering the TDMAZ inlet tube during the fluidization test. Over-fluidization in the zirconia-silica tests resulted in an approximately 1% particle loss from the reactor vessel. The tungsten particles fluidized in clusters, over time the particles would randomly drop from the reaction vessel or over-fluidized into the particle trap in small groups.

4.2 FB-CVD Experiments with Quartz Spouted Fluidized Bed

Table 5 summarizes coating experiments carried out using the quartz vessel (Section 3.1). These initial experiments were performed without a fluidized powder bed. Instead, long metal wires were inserted into the system for diagnostic measurements. The wires used included two 0.7 mm diameter, 300 cm long molybdenum wires, and a 2 mm diameter tungsten wire, 300 cm in length. The length was chosen so that the wires would rest at the bottom of the coated particle trap and extend out of the top outlet of the spouted reaction vessel. The wires did not considerably move vertically during the tests since they were stabilized at the bottom of the particle trap. The location within the vessel where the deposition occurred could be approximated by examining the wire at the conclusion of each experiment.

Table 5. Test Conditions Using Quartz Spouted Fluidized Bed

Test Section	Vessel	Substrate	Heater Temperature °C	High Ar Flow (L/min)	Low Ar Flow (ml/min)	System Operation Time (hrs)	Coating Observed (Y/N)
4.2.1	Quartz	Mo wire	425 ± 75	4.7 ±0.2	60 ± 2	3	Y
4.2.2	Quartz	Mo wire	325 ± 50	4.7 ±0.2	60 ± 2	2.25	Y
4.2.3	Quartz	W Wire	325 ± 50	4.7 ±0.2	60 ± 2	5	Y

4.2.1 Molybdenum Wire Experiment 1

Research performed by W.-I. Kim et al. found that TDMAZ produced coatings between temperatures of 150°C to 350°C in a static low pressure system [18]. The fluidized system will operate at atmospheric pressure which is expected to require a

higher operating temperature to increase coating rate deposition. The first experiment was set up to find the upper temperature bound for the system.

Three thermocouples were set in the furnace used to heat the reaction vessel, one at the top, one at the center and one at the bottom. The temperature of the furnace was set to 425°C, but the temperature was found to fluctuate ± 35°C from the set point and ± 75°C, over the vertical length of the furnace. The precursor bubbler temperature was maintained above the melting temperature of the crystals, at 70 ± 2 °C. During operation a white vapor was observed flowing from the precursor bubbler to the reaction vessel (Fig. 21).

Fig. 21. Precursor bubbler during experiment operation.

Towards the end of the experiment, the digital readout on the mass flow rate from the ammonia controller fluctuated between values of 14.4 mL/min to 89 mL/min, it

was unknown whether the fluctuation was a malfunction of the digital screen or the mass flow controller itself. (It was later determined that the controller was broken and no ammonia was flowing during these initial tests). When vapor was no longer evident leaving the precursor bubbler, the experiment was shut down. The experiment operated for a total of 3 hours.

The furnace was allowed to cool to room temperature before the vessel and the molybdenum wire were removed. The vessel had a dark brown, flakey coating at the main gas inlet and the bottom half of the vessel. The molybdenum wire pictured in Figs. 22 and 23 had the same type of coating, ranging from a flakey brown coating (Fig. 22) corresponding to the inlet of the spouted bed reactor to a more homogeneous dark brown coating corresponding to the center of the reaction vessel (Fig. 23).

Fig. 22. Molybdenum wire coated in the quartz vessel at 425°C; section from the inlet of the spouted bed reactor.

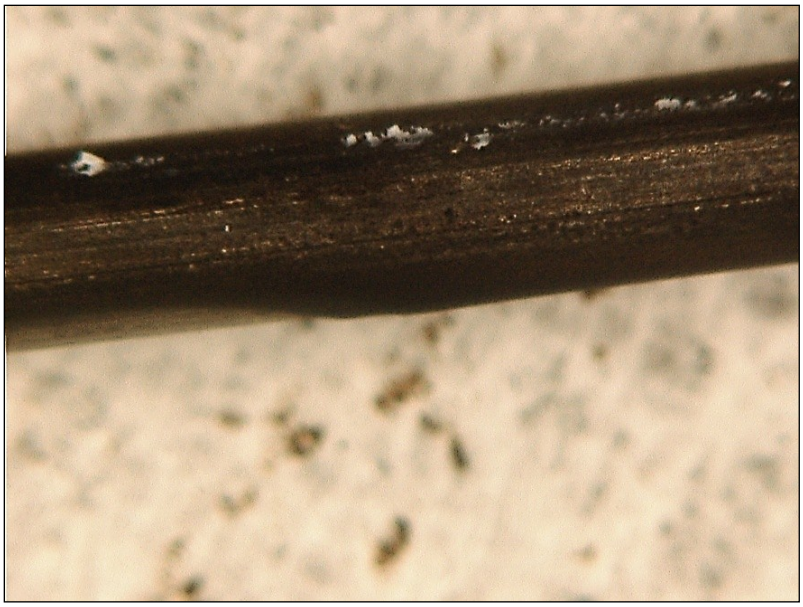

Fig. 23. Molybdenum wire coated in the quartz vessel at 425°C; section from the center of the spouted bed reactor.

The bubbler used to vaporize the TDMAZ crystals still contained most of the precursor when removed from the system. When cooled to room temperature, the leftover precursor did not return to the original white-yellow color, but had changed to a semi-transparent dark orange color.

4.2.2 Molybdenum Wire Experiment 2

The second wire experiment proceeded with the furnace temperature set at 350°C. The furnace midline temperature ranged between 325 ± 50°C. The ammonia mass flow controller digital readout remained stable during this test at 63 ± 5 mL/min. The experiment operated until the precursor vapor was no longer observed exiting the bubbler for a total operation time of 2.25 hours.

The vessel was removed from the furnace after cooling to room temperature and was light golden-brown in color and the wire color ranged from light brown, to golden brown, to an iridescent blue (Fig. 24).

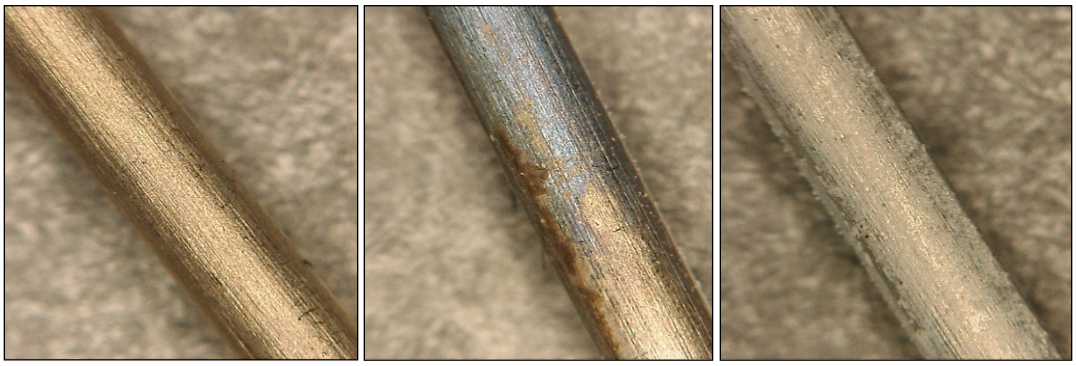

Fig. 24. Molybdenum wire experiment 2; (left) coating location 4" above the spouted bed, (center) coating location 6" above the spouted bed, (right) coating location 14" above the spouted bed.

The wire was examined along the length and an apparent transition was found toward the top of the reaction vessel in the center picture of Fig. 24. The darker brown coating line in the center picture of Fig. 24 is where the wire was resting again the reactor wall. White crystals were found on the top of the wire, right of Fig. 24, corresponding to a location at the exit of the reaction vessel.

As observed in wire experiment 1, a large amount of precursor remained in the bubbler at the conclusion of the experiment.

4.2.3 Tungsten Wire Experiment

The thin molybdenum wire was difficult to set in epoxy for examination. The wire would invariably shift while the epoxy set so that a clear cross section of the wire was not obtainable. A thicker, 2 mm diameter tungsten wire was chosen for experiment 3. The temperature settings were repeated from the previous molybdenum wire test, but the experiment was allowed to run for 5 hours in an attempt to completely vaporize the precursor crystals. The ammonia mass flow controller began to malfunction during the experiment; the digital readout values fluctuated between -19 mL/min to 72 mL/min.

The tungsten wire was removed from the reaction vessel at the conclusion of the experiment; the reaction vessel color varied from a light golden to a golden brown color and the wire color varied from a bright gold to a pink gold color (Fig. 25). The precursor bubbler still had a large amount of precursor remaining in the bubbler.

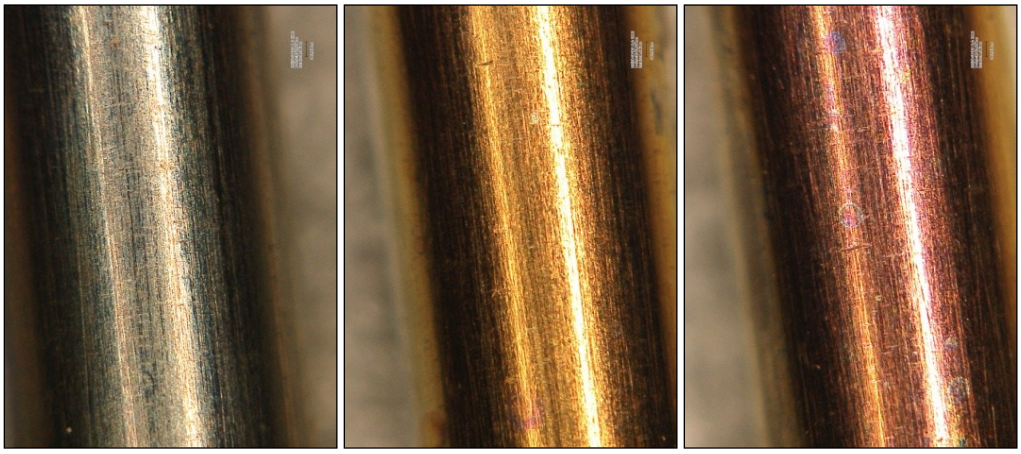

Fig. 25. Tungsten wire coated in the quartz vessel at 325°C at three vertical locations; uncoated surface (left), coated surface (center and right).

4.2.4 Microprobe Characterization of the Coated Wires

Electron microscopy methods did not reveal a measureable coating thickness around the circumference of either wire, indicating the coating thickness was less than ~0.5 µm. WDS analysis on the molybdenum wire from experiment 2 did not find any nitrogen, however, zirconium and oxygen were both present on the wire surface; the oxygen content was much greater than the zirconium (Figs. 26 and 27). EDS analysis on the tungsten wire from experiment 3 found zirconium, oxygen and nitrogen on the wire surface, but the content varied over the length of the wire as shown in Figs. 28 to 30.

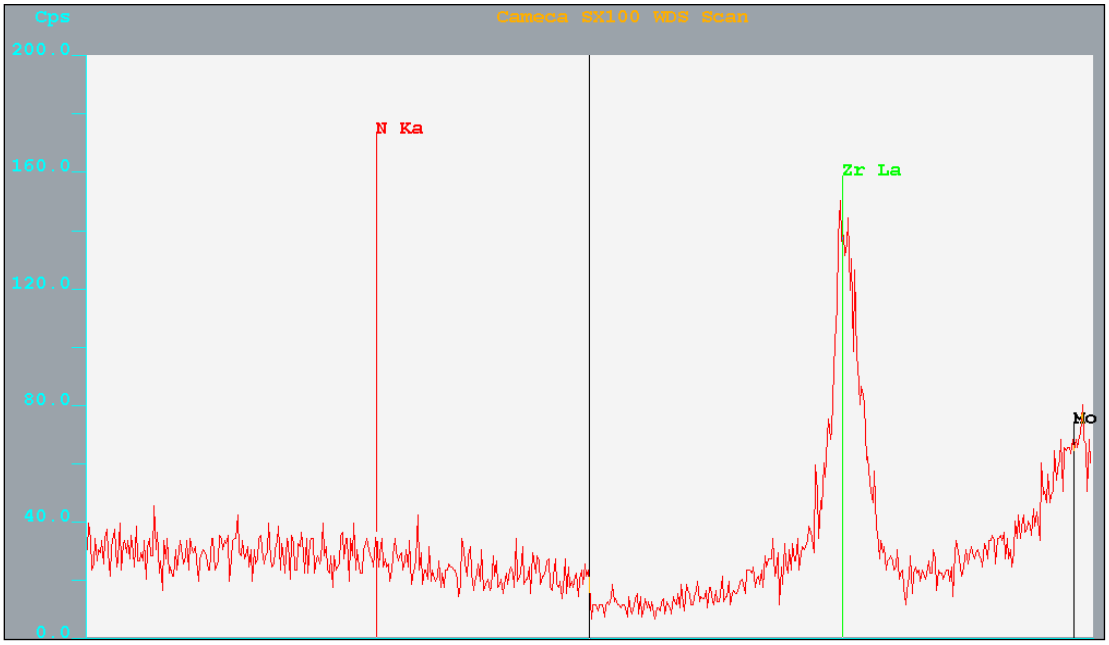

Fig. 26. Wavelength Dispersive Spectroscopy spectrum of coated Mo wire revealing the apparent absence of nitrogen and presence of zirconium.

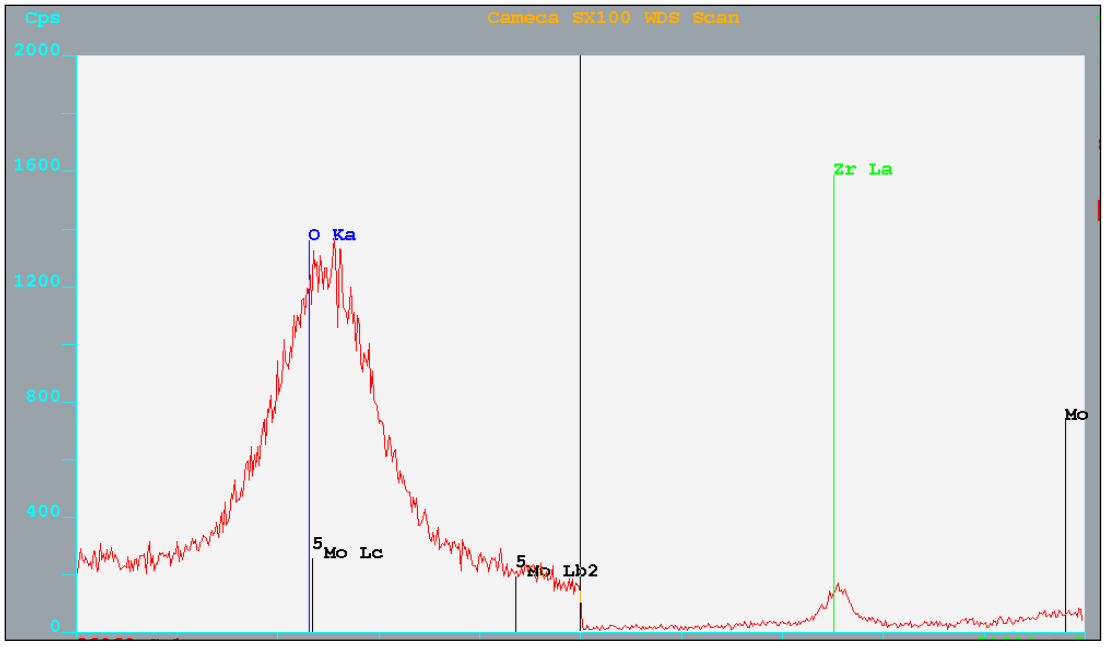

Fig. 27. Wavelength Dispersive Spectroscopy spectrum of coated Mo wire revealing the presence of oxygen and zirconium.

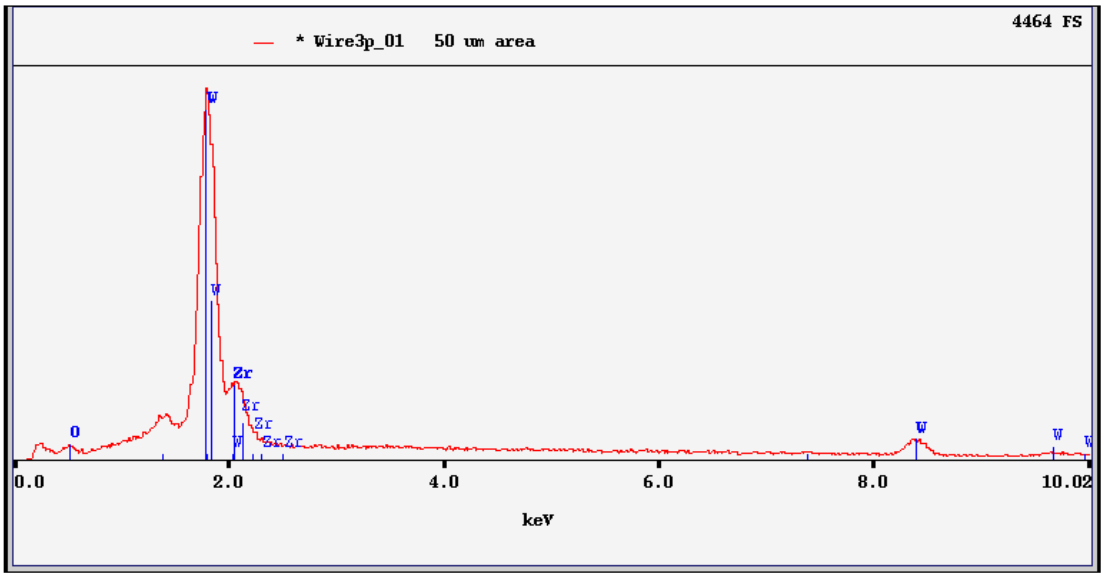

Fig. 28. First Energy Dispersive Spectroscopy of wire experiment 3, oxygen and zirconium content.

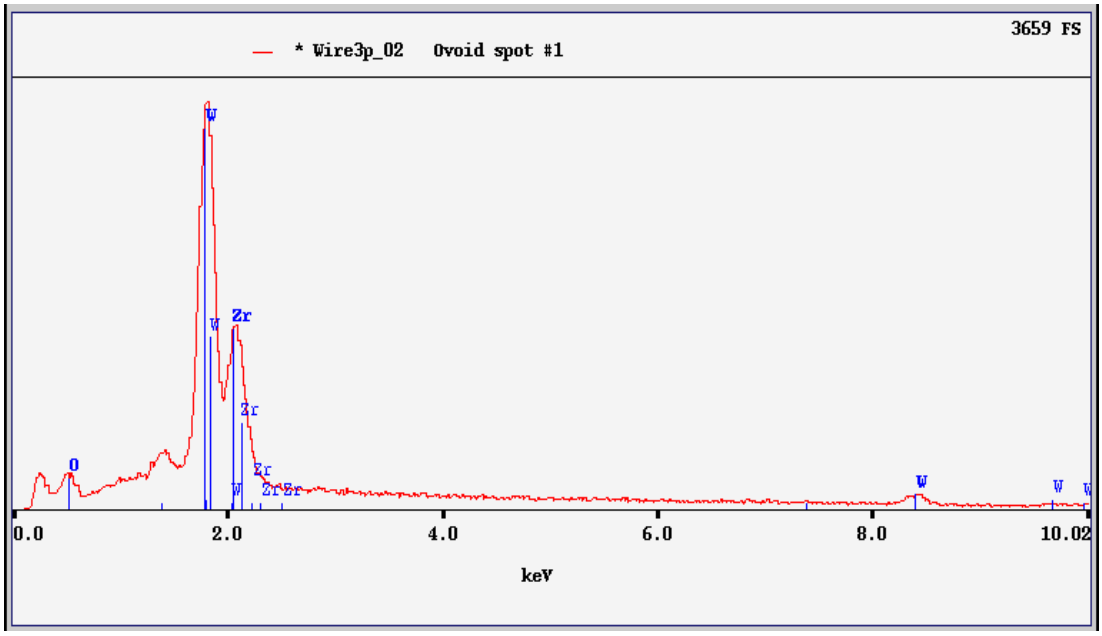

Fig. 29. Second Energy Dispersive Spectroscopy of wire experiment 3, oxygen and zirconium content.

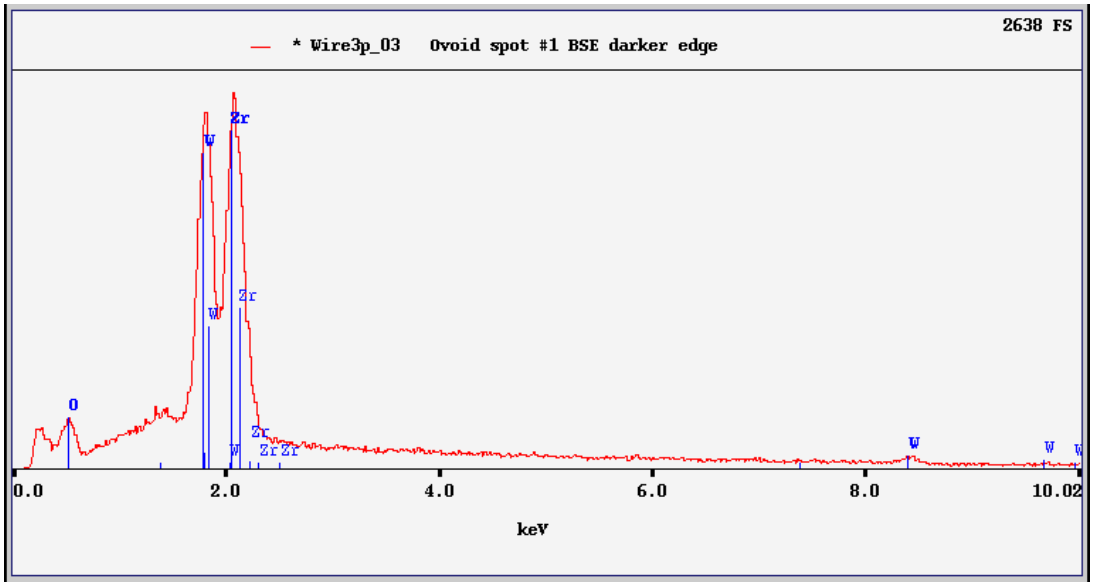

Fig. 30. Third Energy Dispersive Spectroscopy of wire experiment 3, oxygen and zirconium content.

4.2.5 Quartz Fluidized Bed Results Summary

The size and shape of the quartz vessel successively fluidized different sizes and shapes of particles (Section 4.1) and the CVD system successfully deposited coatings onto the wire substrates (Section 4.2). The deposited coating on the wires was too thin for thickness measurements so the process parameters required further modifications to optimize the deposition rate.

One notable observation is that the quartz vessel was exceptionally brittle and cracked easily during insertion and removal from the experiment system. The vessel continually had to be repaired, which increased time in between experiments. The repairs on the reactor were not always exact and connecting the quartz inlets to the steel tubing lines required modifications of the stainless steel tubing length and connection angles (Fig. 31).

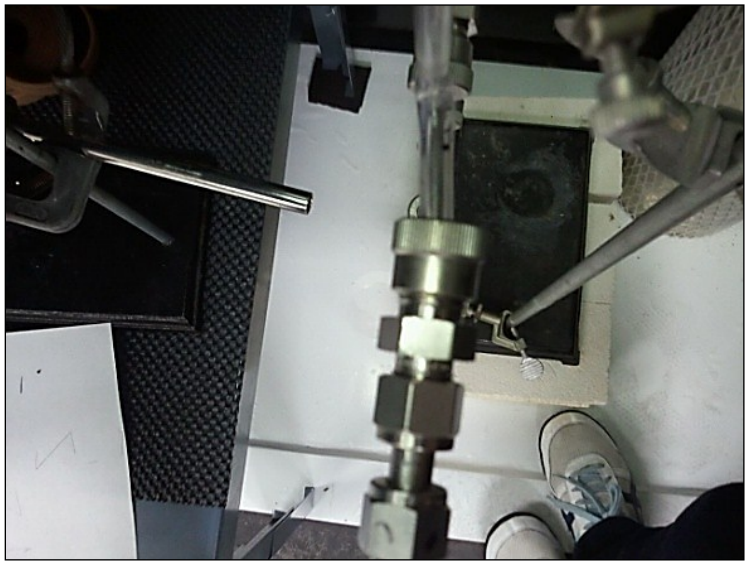

Fig. 31. Misaligned glass inlet connection after repairs to the reaction vessel.

The vessel design was modified to include a powder inlet and was created from Pyrex glass, which is much less brittle than quartz. The vessel dimensions were matched to the quartz vessel in terms of same spouted bed cone angle and reactor diameter and length.

Difficulties with vaporizing the precursor using the bubbler prompted a redesign of the bubbler as well. The new bubbler (Section 3.1.1) was designed to fluidize the solid TDMAZ precursor with the carrier gas by running the carrier gas underneath the crystals through a fritted plate to ensure maximum contact between the crystals and heated gas, theoretically increasing the vaporization rate.

4.3 FB-CVD Experiments with Pyrex Spouted Fluidized Bed

The Pyrex vessel components (Section 3.1.1), the redesigned bubbler (Section 3.1.1), and a new mass flow controller for the ammonia stream were installed for the next set of experiments. Alloy microspheres U-7Mo (natural uranium) were received from INL and utilized for the following coating experiments. The diameter of the microspheres ranged from 45 μm to 125 μm. The U-7Mo particles were separated by size using a sieve shaker. The size range used for the following experiments was (75 μm < x < 125 μm. Fig. 32 is a picture of the U-7Mo particles within the reaction vessel, prior to being released into the fluidized bed. Table 6 summarizes the process conditions for each experiment discussed in this section; note that coatings were never observed using this configuration.

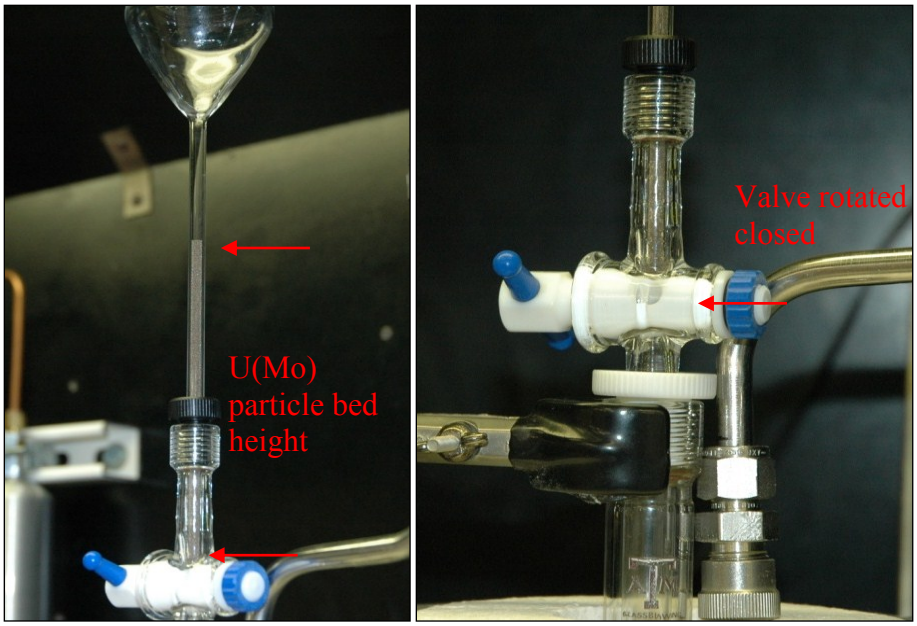

Fig. 32. U-7Mo experiment using the top loading Pyrex spouted bed reactor.

Table 6. Test Conditions Using Pyrex Spouted Fluidized Bed

Test Section	Vessel	Substrate	Heater Temperature °C	High Ar Flow (L/min)	Low Ar Flow (ml/min)	Precursor (grams)	Coating Observed (Y/N)
4.3.1	I: Pyrex	U-7Mo	237±25	5.5 ±0.5	60 ± 2	1.5	N
4.3.2	I: Pyrex	U-7Mo	265±25	4.9 ±0.5	60 ± 2	3.01	N
4.3.3	I: Pyrex	U-7Mo	300±25	4.6 ±0.5	60 ± 2	3.3	N
4.3.4	I: Pyrex	U-7Mo	350±25	4.1 ±0.5	60 ± 2	3.32	N

4.3.1 U-7Mo Experiment 1

The total operation time for the U-7Mo experiment 1 was 3 hours; the experiment was shut down when precursor vapor was no longer evident from the precursor bubbler. The microspheres fluidized at 5.5 L/min but some of the

microspheres were over-fluidized into the particle trap. At the conclusion of the experiment, the reaction vessel was uncoated although a fine yellow powder was evident in the particle trap connected to the exhaust exit of the reaction vessel. Visual inspection of the microspheres was inconclusive as U-7Mo particles range in color from bronze to blue (Fig. 33) and the nearly identical color variation is expected with or without the ZrN coatings, depending on oxygen content in the coating [23].

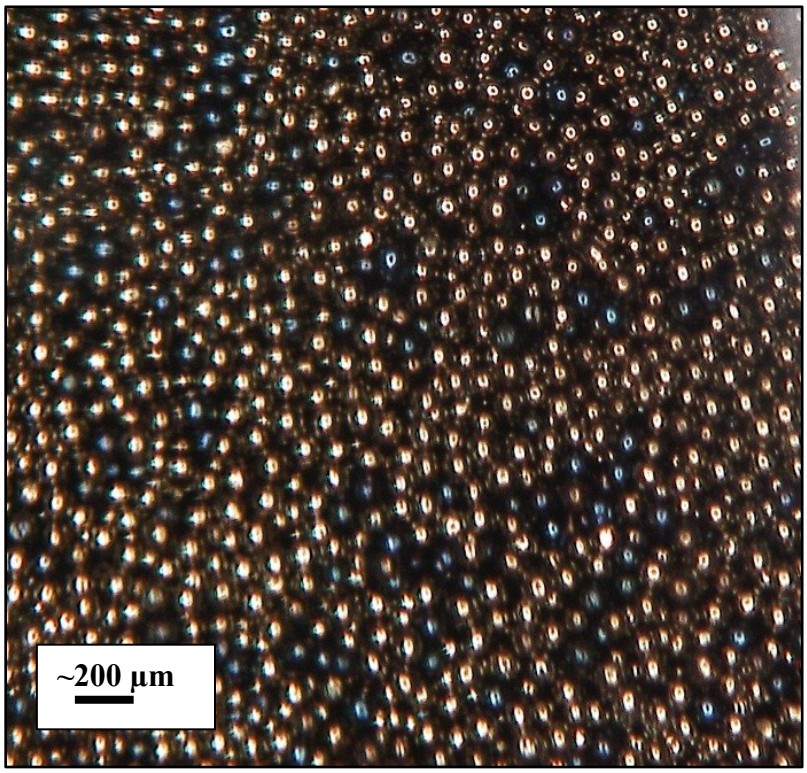

Fig. 33. Original uncoated U-7Mo microspheres.

4.3.2 U-7Mo Experiment 2

The system temperature for the U-7Mo experiment 2 was raised to 265 ± 25°C and the total operation time for the was 2.25 hours. The microspheres fluidized at 4.9L/min but some of the microspheres were over-fluidized out of the vessel and into the particle trap. At the conclusion of the experiment, the reaction vessel was uncoated although the microspheres now appeared a maroon-bronze color instead of the original golden bronze color. Again the fine yellow powder was evident in exhaust lines and the particle trap.

4.3.3 U-7Mo Experiment 3

The system temperature for the U-7Mo experiment 3 was raised to 300 ± 25°C and the total operation time was 45 minutes. The microspheres fluidized at 5.3 L/min. Forty-five minutes into the experiment, the high purity argon tank emptied and the particles fell into the coated particle trap. The reaction vessel was uncoated when removed from the furnace and no visible color change was noted for the U-7Mo microspheres.

4.3.4 U-7Mo Experiment 4

The system temperature for the last U-7Mo experiment was 350 ± 25°C and operated for a total time of 3 hours. The microspheres fluidized at an argon flow of 4.1 L/min with a small fraction of the microspheres overfluidizing into the particle trap. The reaction vessel was uncoated when removed from the furnace, the yellow powder

was found in the exhaust tubing leading from the reaction vessel, and no visible color change was noted for the U-7Mo microspheres.

4.3.5 Microprobe Characterization

The microspheres were difficult to polish due to the difference in hardness between the epoxy and U-7Mo. Aggressive polishing pulled the microspheres from the epoxy and light polishing rounded the edge of the microspheres, inhibiting the confirmation of the presence or absence of a coating layer. Loose microspheres were attached to carbon tape and WDS used to detect the elements of interest on the surface of the spheres.

WDS analysis did not find any traces of zirconium on the spheres. Elevated nitrogen content was found on the microspheres that had changed to a maroon color, but the reason for the increased nitrogen content is unknown.

4.2.5 Pyrex Fluidized Bed Results Summary

The bronze color of the U-7Mo microspheres made it difficult to visually inspect the powder for a coating at the conclusion of each experiment and the radioactive nature of the microspheres increased the hazards associated with the preparation, cleanup, and maintenance of the system. The zirconia-silica microspheres in the lab were chosen as a surrogate for the U-7Mo fuel particles. Unlike the tungsten powder, the zirconia-silica were round in shape and easily fluidized. The white color faciliated visual coating inspections without having to take the samples to the EPMA and the microspheres were

not radioactive, making the system operation and clean up much easier. After coating process conditions are verified, the U-7Mo particles will be used as the substrate in subsequent experiments.

Precursor evaporation continued to be a problem with the new fritted plate bubbler. At the conclusion of each experiment in this section, most of the precursor was still found within the bubbler vessel. Cleaning the fritted bubbler required the use of pirahna acid (three parts sulfuric acid to one part hydrogen peroxide) which is a hazardous and lengthly process. A smaller, stainless steel bubbler was created to replace the glass bubblers (Section 3.2). The bubbler was easy to load and clean and could be placed three feet closer to the reaction vessel to reduce the length of tubing the vaporized precursor travelled.

Fluidization concerns prompted the redesign of the fluidized bed reactor (Section 3.2). Although fluidization was demonstrated as effective for the spouted bed design, particle loss still occurred during operation. A portion of the fluidized powders was always lost from the spouted bed, either smaller over-fluidized particles leaving through the exhaust tubing or larger under-fluidized particles falling through the inlet. Lower fluidized particles would not have the same theoretical uniform coating as the particles within the fluidized bed and particles collected at the conclusion of each experiment could have a mixture of coating thicknesses and possibly some particles that remained uncoated. Also, the U-7Mo particles had to be transported in an inert gas from the glovebox to the experiment system. Detaching and reattaching the glass containment vessel at the top of the reaction vessel was difficult and resulted in glass fractures. Each

time a vessel port fractured, the experiment progress was halted as time consuming repairs were made. A new fluidization vessel was needed that was compact, could transport the coated and uncoated particles, and would keep all the particles within the reaction zone. The vessel would preferrably have all tubing to vessel connections made from steel while the vessel itself was glass for obervation during coating experiments. The inverted fluidized bed vessel discussed in Section 3.2 was created and built to meet the above criteria.

The complete evaporation of the TDMAZ precursor continued to be an issue. Only 7 to 10% (by mass) of the precursor loaded was evaporated during each system operation. The evaporation of solid precursors is problematic for many CVD systems and it has been shown that when the precursor is heated for an extended period of time, it can begin to decompose and polymerize into non-volitile resides [28]. To avoid decomposition of the precursor, the bubbler was heated below the melting point of the precursor crystals in the next set of experiments (Section 4.4).

As another significant observation, it was noted that ZrN coating can be achieved using the TDMAZ precursor without ammonia [27]. The purpose of the ammonia in CVD experiments in literature was to reduce carbon contamination of the resultant coatings [8]. Ammonia and TDMAZ will react even at low temperatures and the observed yellow powder in the outlet traps suggested that the ammonia reacted with the precursor prior to exiting into the reaction chamber. Therefore, the procedures for the next set of experiments was modified to operate without ammonia first and then to slowly introduce small amounts of ammonia into the system.

4.4 FB-CVD Experiments with Inverted Fluidized Bed

Table 7 summarizes the process conditions for each experiment discussed in this section. These experiments were completed with the inverted fluidized bed reactor (Section 3.2) using argon gas and the TDMAZ precursor. The ammonia gas was omitted from all the experiments with the exception of test 4.3.2. These experiments were performed using the zirconia-silica microspheres (185-250 μm) as substrates for the coating process. This was done, in part, to remove the complication of working with radioactive materials while perfecting the coating process and, in part, to have contrast between the white spheres and the coated particles. The TDMAZ precursor melting point is 58°C [18, 27], so the precursor was heated to 51 ± 2°C for each experiment. The furnace was replaced with an aluminum annulus, 20.31 cm (8 in) in length, heated with fiberglass heater tape. The temperature of the new heater did not fluctuate as the furnace did, making the system operations more reliable. The vessel contents were periodically monitored by lifting the annulus during system operation.

Table 7. Test Conditions Using Inverted Fluidized Bed

Test Section	Vessel	Substrate	Heater Temperature (°C)	High Ar Flow (L/min)	Low Ar Flow (ml/min)	Operation Time (hrs)	Coating Observed (Y/N)
4.4.1	Inverted	zirconia–silica	237 ± 5	1.0 ± 0.5	95 ± 2	4	Y
4.4.2	Inverted	zirconia–silica	250 ± 5	1.0 ± 0.5	95 ± 2	4	Y
4.4.3	Inverted	zirconia–silica	265 ± 5	1.0 ± 0.5	95 ± 2	18	Y
4.4.4a	Inverted	zirconia–silica	255 ± 5	1.0 ± 0.5	95 ± 2	10	Y
4.4.4b	Inverted	zirconia–silica	210 ± 5	1.0 ± 0.5	95 ± 2	12	N
4.4.5	Inverted	zirconia–silica	280 ± 5	1.0 ± 0.5	95 ± 2	69	Y

4.4.1 Fluidization Tests for the Inverted Fluidized Bed

Fluidization tests were performed using the tungsten particles (Fig. 34) and the zirconia–silica microspheres (Fig. 34). The tungsten particles successfully fluidized within the reaction vessel. However, some smaller, irregularly shaped particles were fluidized to the top of the vessel. Particles fluidized outside the heated zone of the vessel are not expected to have as uniform a coating as those fluidized within the heated zone. The tungsten particles were not utilized for the experiments reported in Section 4.3.

Fig. 34. Fluidization of tungsten particles in the inverted fluidized bed system.

The zirconia-silica particles fluidized at a high argon flow rate of 1.0 ± 0.5 L/min and a low argon flow rate of 95 ± 2 mL/min, when the bed of particles became fully expanded. These two flow rates were used for all the experiments reported in Section 4.3.

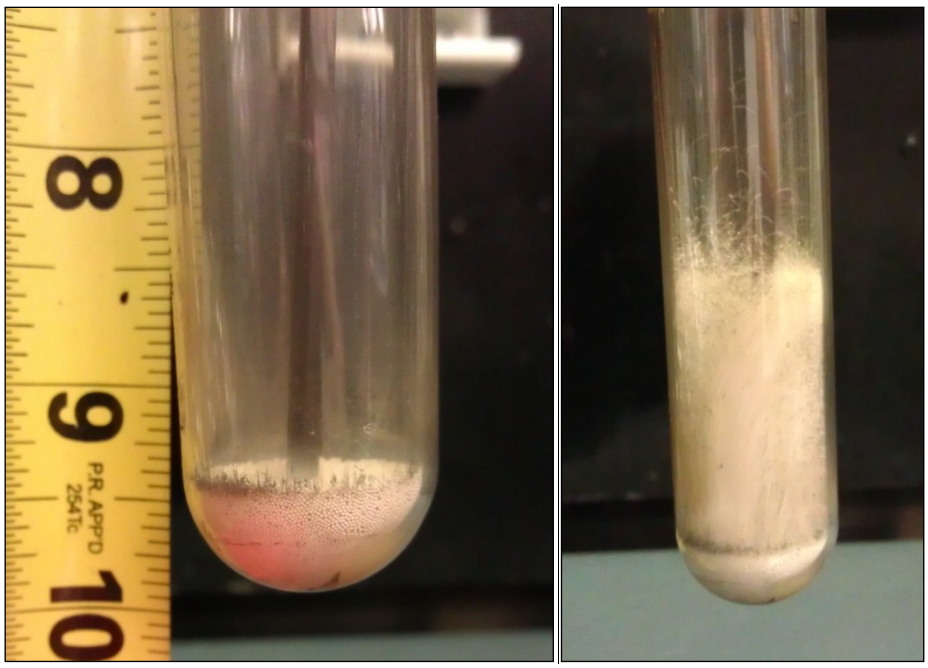

Fig. 35. Fluidization of zirconia-silica particles in the inverted fluidized bed system, static bed (left) and fully expanded bed (right).

The heated aluminum annulus was setup so that only the bottom 15.25 cm (6 in) of the 30.5 cm (12 in) reactor was heated during system operation (Fig. 36). This prevented the precursor from heating up too rapidly while traversing the length of the gas inlet to the bottom of the reaction vessel. The annulus could slide up the length of the vessel, exposing the fluidized bed at the bottom, enabling periodic fluidization checks during system operation.

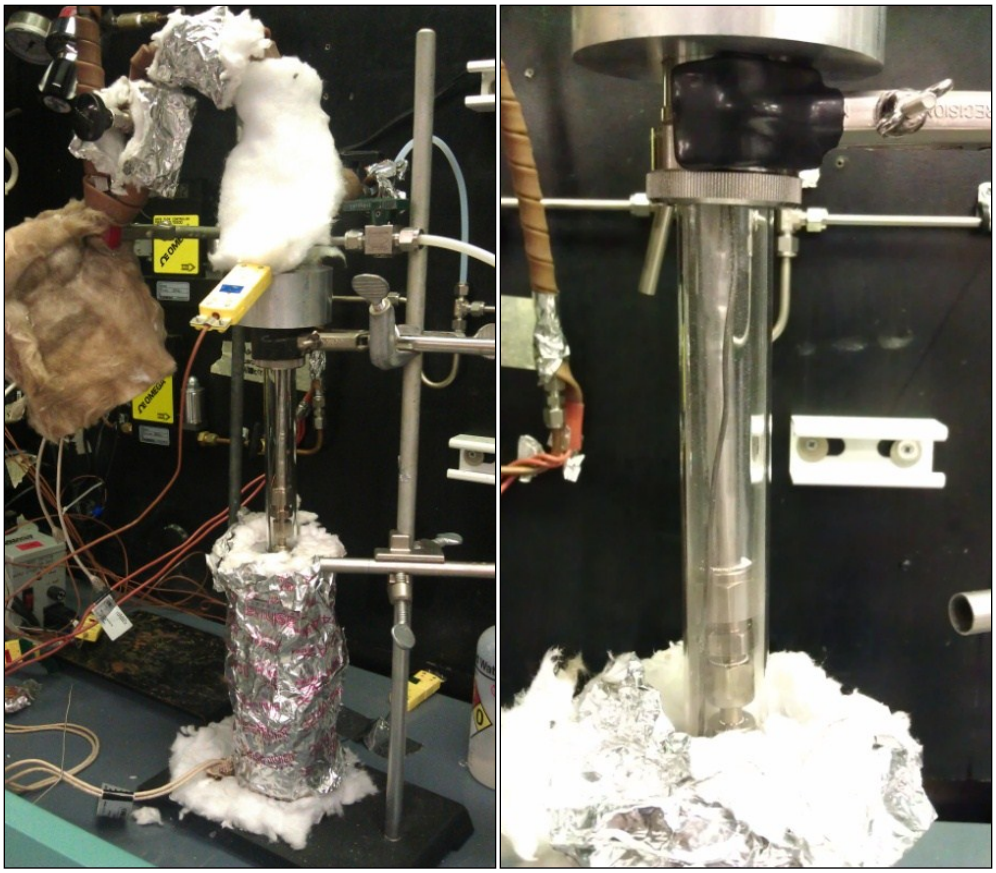

Fig. 36. Inverted fluidized bed reactor in operation.

4.4.2 Zirconia–Silica Experiment 1

The first zirconia–silica experiment was operated for a total of 4 hours. The particles remained fluidized within the reaction vessel without any over-fluidizing into the particle trap and the temperature over the length of the vessel only changed by 5°C. At the conclusion of the experiment, the reaction vessel was coated a light golden brown. The microspheres were also light golden brown in color. Figure 37 compares the coated microspheres to the uncoated white microspheres.

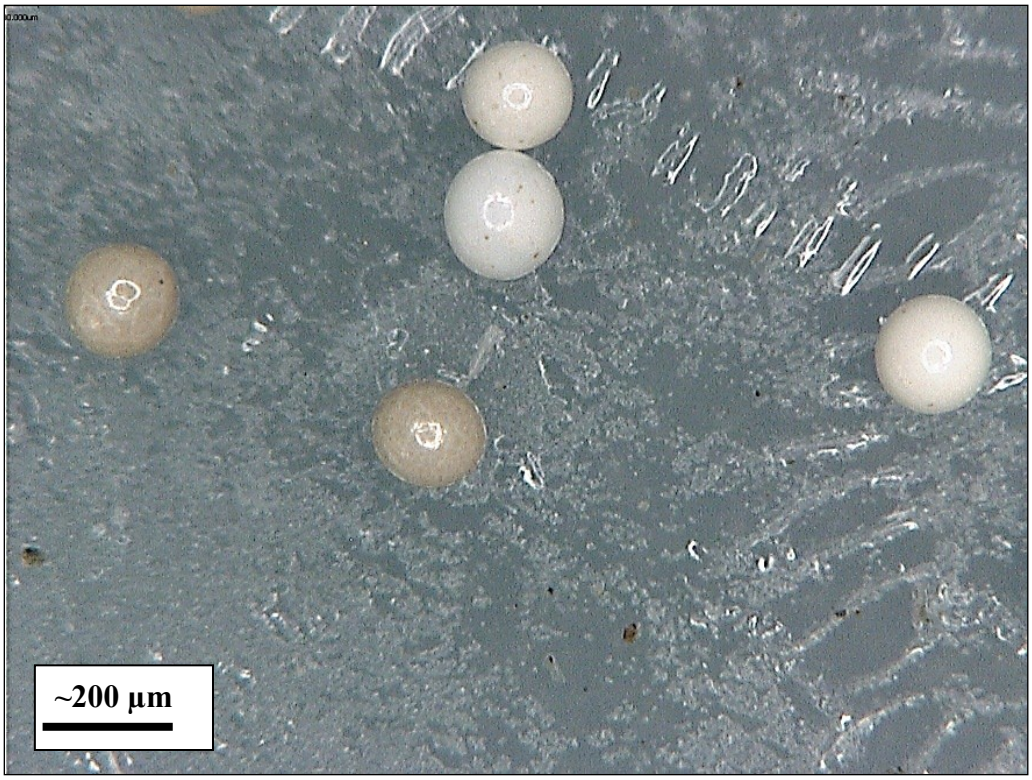

Fig. 37. Zirconia-silica microspheres from experiment 1 (the uncoated spheres were added for contrast).

4.4.3 Zirconia–Silica Experiment 2

The second experiment matched the conditions of experiment 1 except that a small amount of ammonia, 10 mL/min, was introduced into the system. At the conclusion of the experiment, the reaction vessel was uncoated and the microspheres were a speckled off-white color (Fig. 38). The tubing leading from the reaction vessel contained an off-white powder as observed before in the Section 4.3 experiments. Apparently, the ammonia was detrimental to coating formation and the ammonia gas was omitted from the remainder of the Section 4.4 experiments.

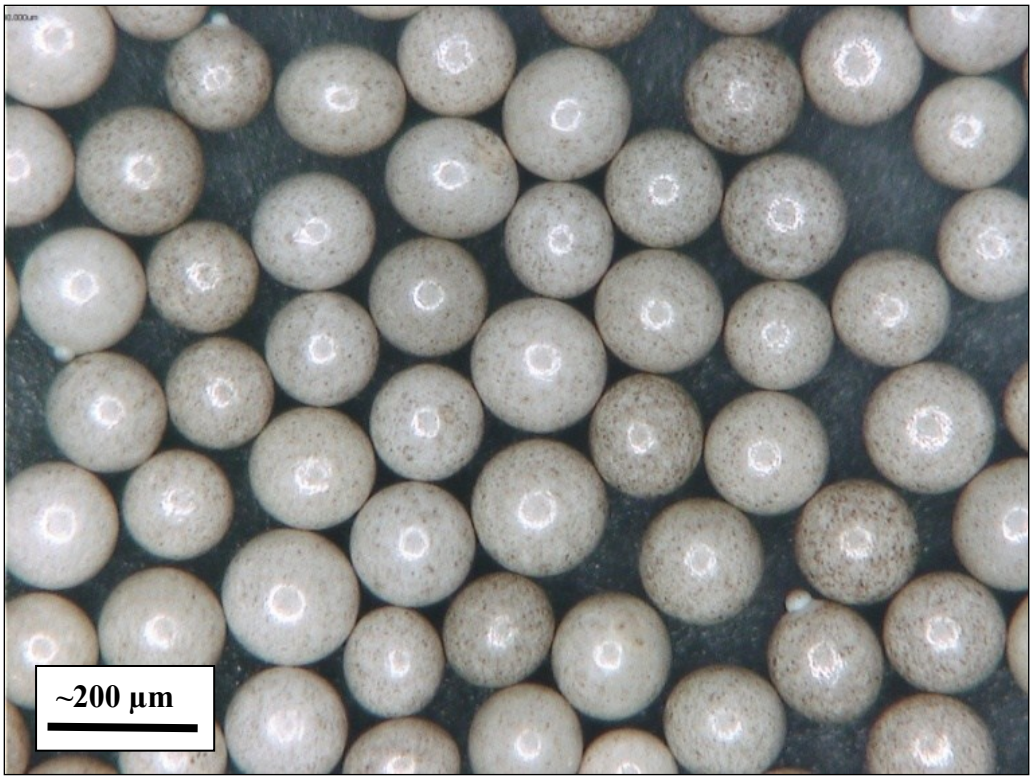

Fig. 38. Zirconia-silica microspheres from experiment 2.

4.4.4 Zirconia–Silica Experiment 3

The third experiment proceeded with a system temperature of 260 ± 5°C and operated for 18 hours before shutdown. The vessel was now a darker iridescent brown color and the microspheres collected were darker in color than those from experiment 1. Figure 39 compares the experiment 3 particles with an uncoated particle.

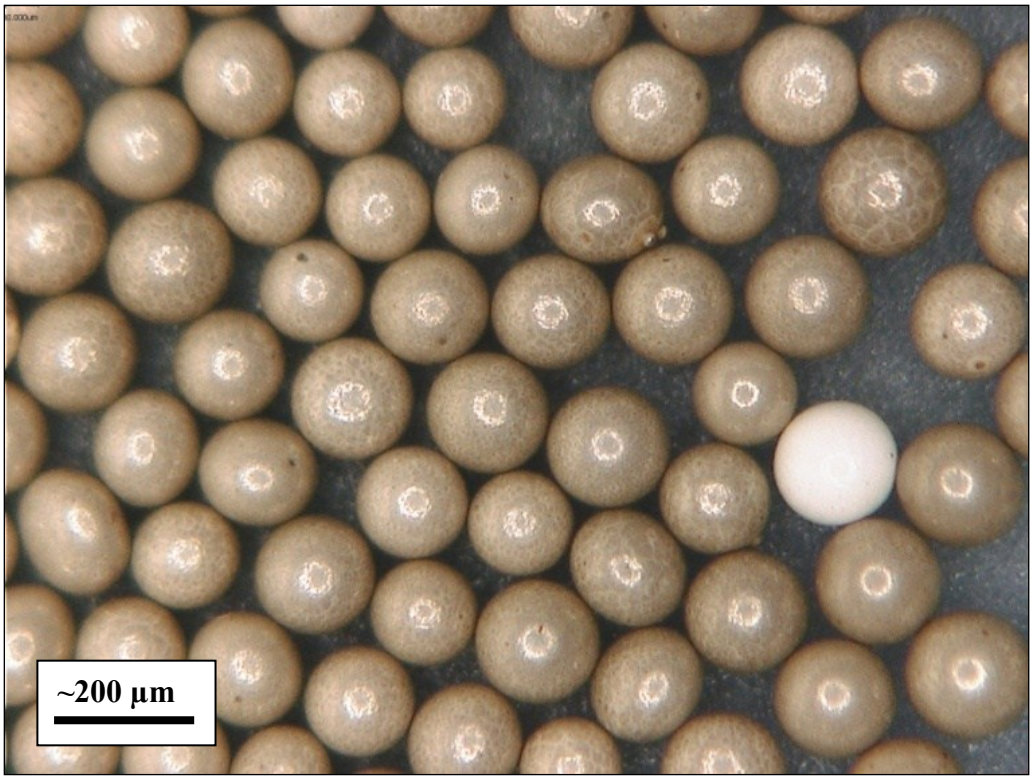

Fig. 39. Zirconia-silica microspheres from experiment 3 (the uncoated sphere was added for contrast).

4.4.5 Zirconia–Silica Experiment 4

The fourth experiment was intended to match to condition of the third experiment but to double the system operating time. The experiment proceeded with a system temperature of 250 ± 5°C and operated for 10 hours before a malfunction of the argon mass flow controllers required a system shutdown. A sample the microspheres were collected and labeled experiment 4a (Fig. 40) and the system was reset with the remaining microspheres. The precursor bubbler was isolated during the system reset but since the precursor had possible air contamination, the remainder of the precursor was used to see if the lower temperature bound could be found for the coating experiments.

The system temperature was set to 210 ± 5°C and restarted for the second half of experiment 4.

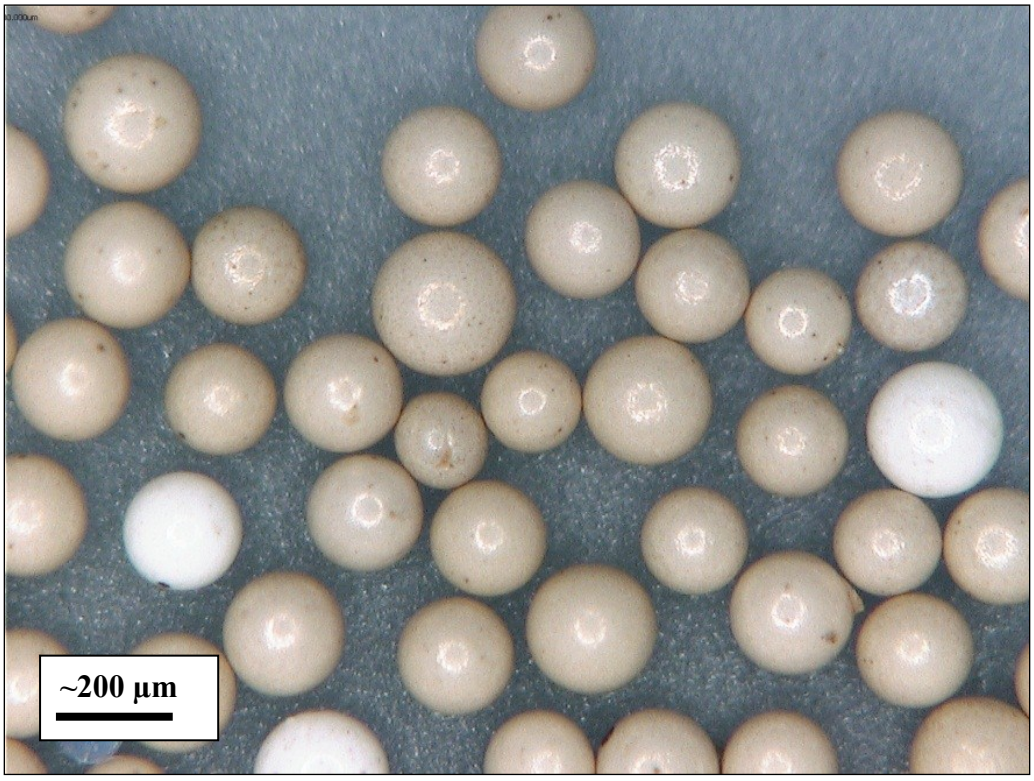

Fig. 40. Zirconia-silica microspheres from experiment 4a (the uncoated sphere was added for contrast).

After 12 hours, the reaction vessel was checked; the precursor had condensed on the top half of the reaction vessel and no evidence of coating was found on the inside of the vessel (Fig. 41). This indicates that the conditions used for Experiment 4b were below the threshold for effective coating.

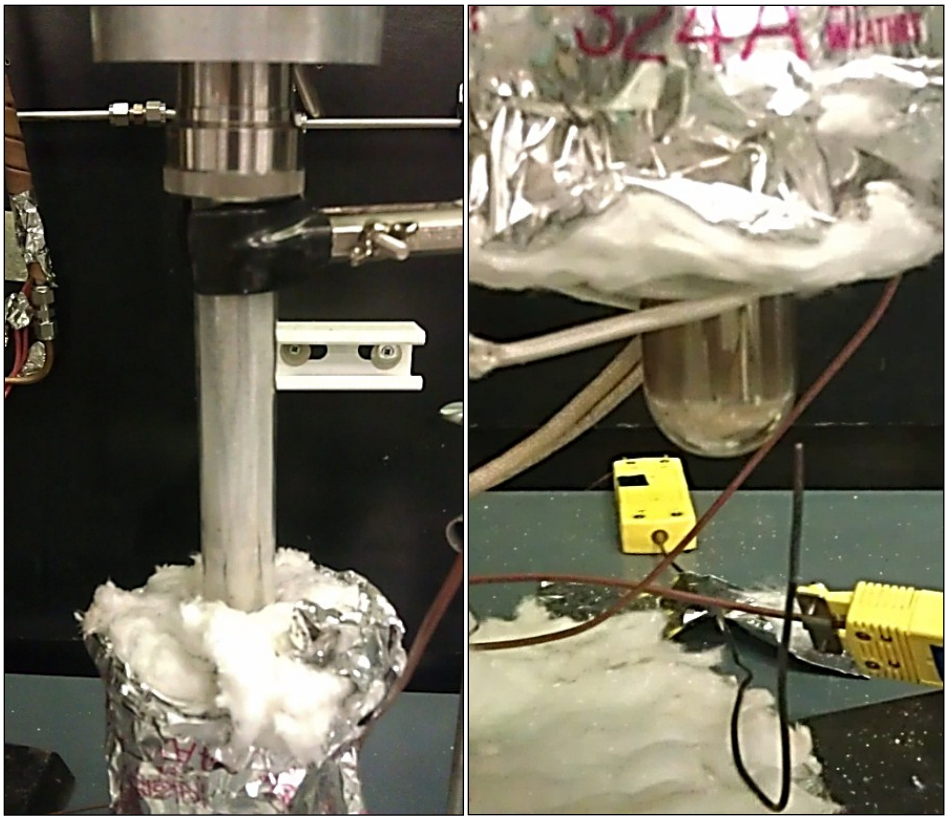

Fig. 41. Reaction vessel from experiment 4b.

4.4.6 Zirconia–Silica Experiment 5

The fifth experiment was run in an uncoated vessel at a temperature of 280 ± 5ºC. Sectioning and polishing the microspheres for analysis at the EPMA up to this point had proven ineffective since the edge of the microsphere tends to round when polished, making coating thickness approximation difficult. In this experiment, a small tungsten wire was placed in the vessel with the microspheres as the larger cross section wire is easier to section and polish without excessive rounding effects.

The experiment operated for 69 hours and the vessel was notably coated at the conclusion of the experiment, as shown in Fig. 42. The picture on the left of Fig. 42

shows the top coated surface of the reaction vessel where the insulation was wrapped. Unheated sections of the vessel above the heated zone are uncoated. The picture on the right of Fig. 42 is the reaction vessel removed from the heater showing the uniform coating corresponding to the heated zone of the vessel.

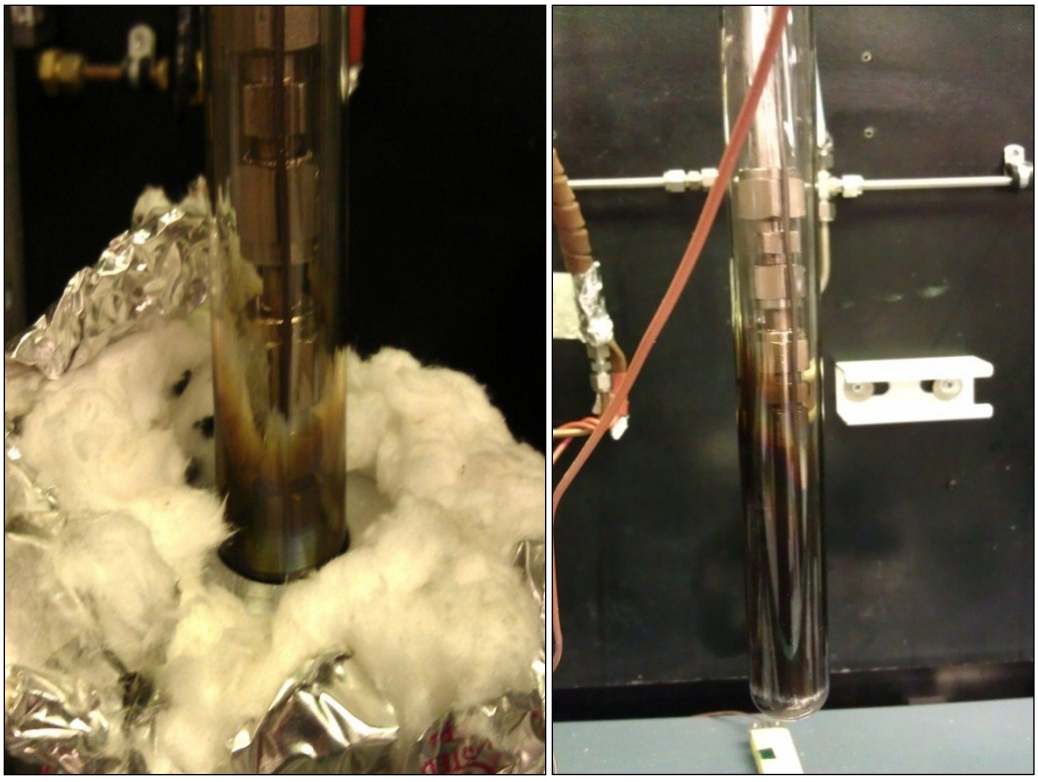

Fig. 42. Coated reaction vessel from experiment 5.

The particles retrieved were dark in color and the wire was a reflective blue color. Figure 43 is an optical image of the experiment 5 particles with uncoated particles for comparison. Fig. 44 is the uncoated tungsten wire (left) next to the coated tungsten wire (right).

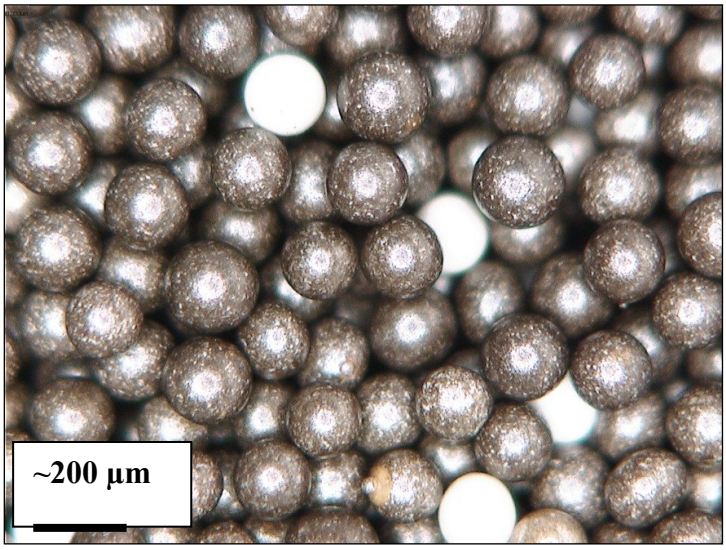

Fig. 43. Zirconia-silica microspheres from experiment 5.

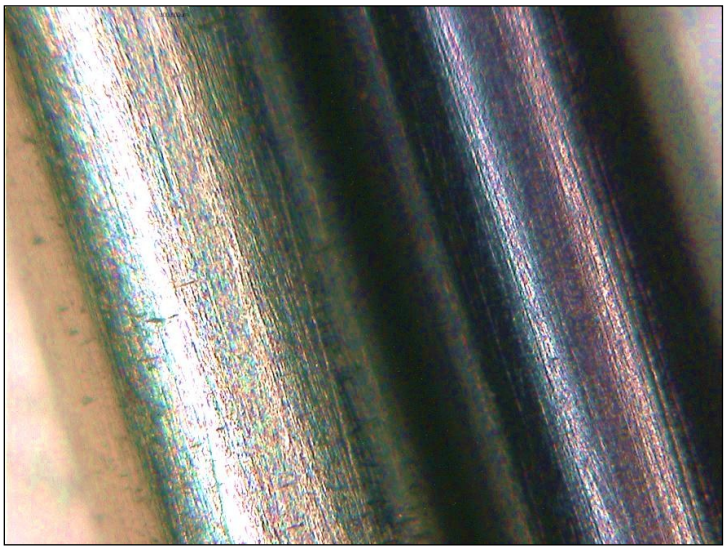

Fig. 44. Tungsten wire from experiment 5 (uncoated on the left, coated on the right).

The microspheres from experiments 3 to 5 and the tungsten wire were placed in epoxy, polished and taken to the Geology EMPA for analysis. Experiment 5 was the final experiment for this portion of the research, so the glass tube used as the reaction vessel was also sectioned and placed in epoxy for analysis. The surfaces of uncoated particles (control) and coated particles from experiments 4a, 3, 5 and the tungsten wire from 5 were also examined.

4.4.7 Microprobe Characterization

The uncoated spheres were examined first to compare to the coated spheres. The uncoated zirconia-silica microspheres are have a porous heterogeneous surface with mixtures of zirconium and silicon, silicon and oxygen, zirconium and oxygen, etc. which can be observed in the BSE image in Fig 45.

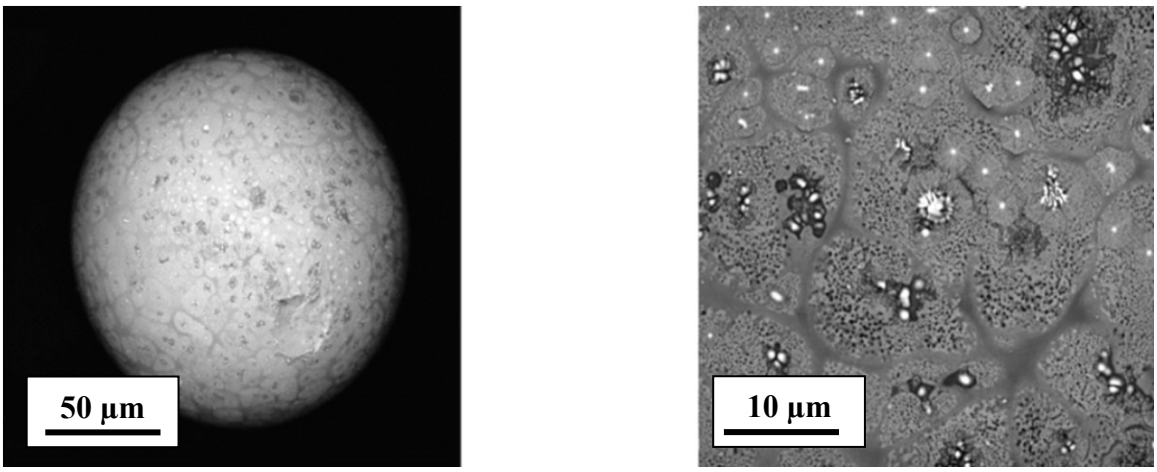

Figure 45. Uncoated zirconia-silica microsphere; the uncoated sphere (left) coupled with a magnified 40 µm surface diameter of the sphere (right).

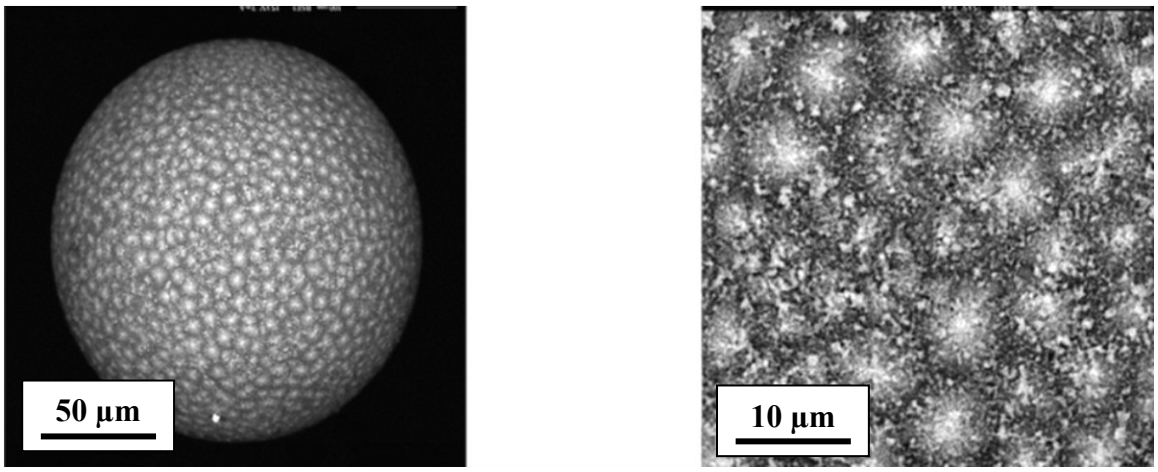

Figure 46. Coated microsphere (left) with the magnified surface (right); Experiment 4a - 10 hours at 265°C.

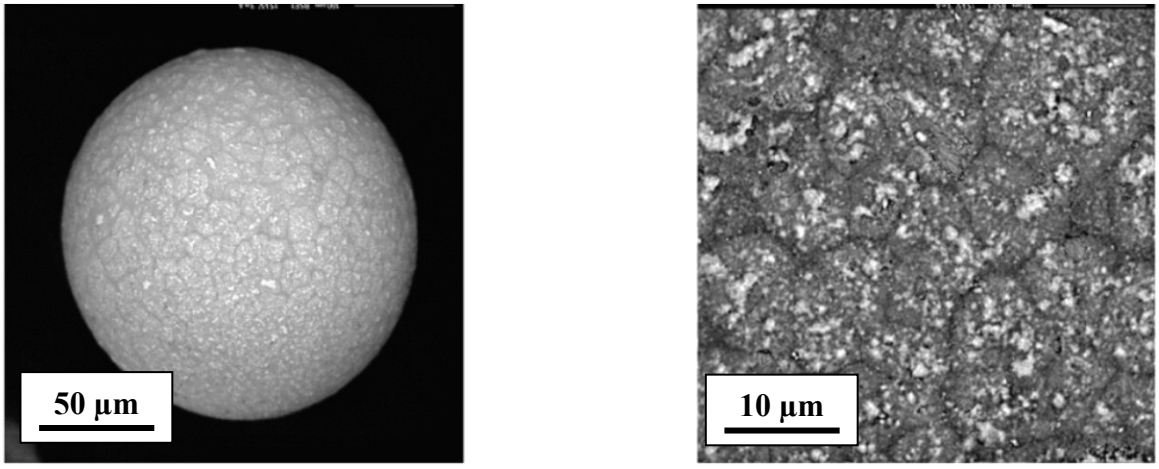

Figure 47. Coated microsphere (left) with the magnified surface (right); Experiment 3 - 18 hours at 255°C.

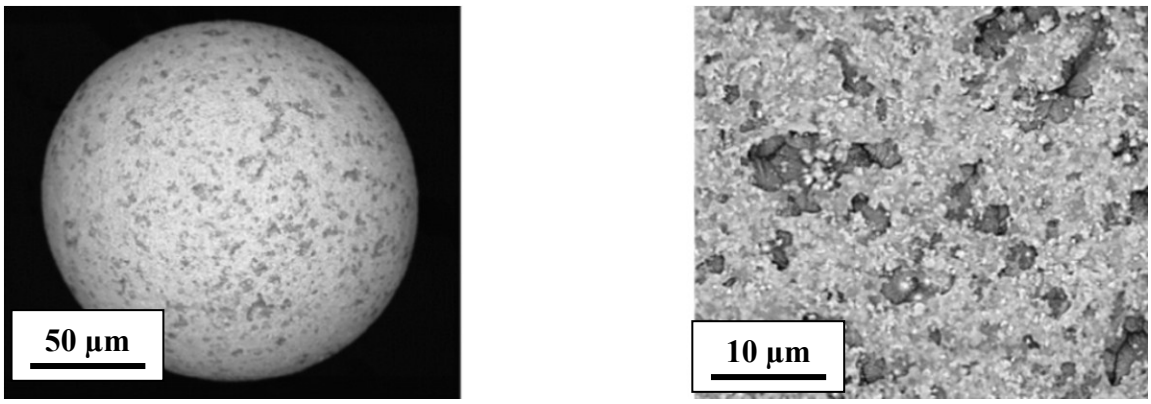

Figure 48. Coated microsphere (left) with the magnified surface (right); Experiment 5 - 69 hours at 280°C.

Figures 46 to 48 are images of the microspheres coupled with magnified 40 µm sections of the sphere surface from experiments 3, 4a and 5 respectively. Each picture shows how the coating nucleates from a specific area of the sphere and grows outward with increased deposition time. The lighter areas in the picture are those with a thicker coating, with experiment 5 showing the thickest coating from the above experiments.

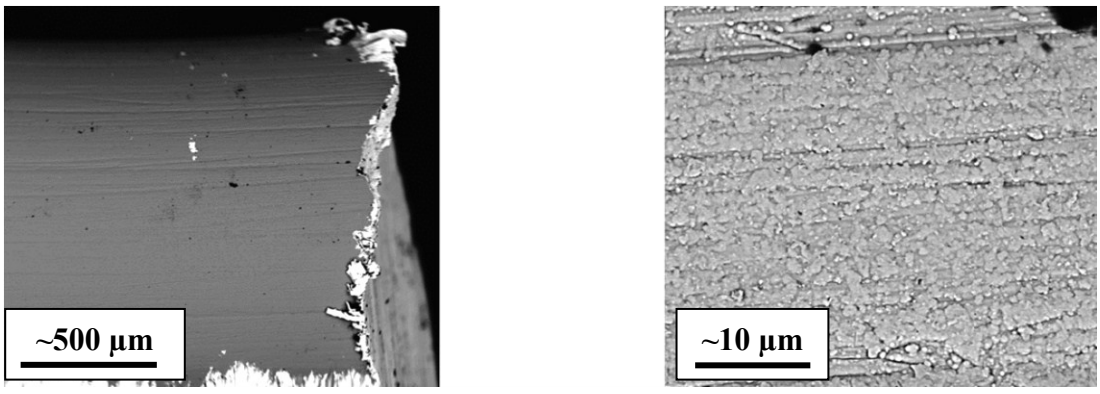

Fig. 49. Coated tungsten wire (left) with the magnified surface (right); Experiment 5 - 69 hours at 280°C.

The BSE images of the tungsten wire are provided in Fig. 49. The picture on the left of Fig. 49 is an image of the end of the tungsten wire where it was sectioned, with the darker areas corresponding to the coated section and the lighter area corresponding to pure tungsten. The coating on the surface of the tungsten wire (Fig. 49 right) is much more uniform than that of the zirconia-silica microspheres.

Images from the section of the tungsten wire that was mounted and polished are provided in Fig 50. The coating was easily visible and varied from 0.5 µm up to 30 µm around the circumference of the wire. The light area is the tungsten wire and the gray area is the coating. The black in between the wire and the coating is from where the epoxy pulled the coating from the wire as it hardened.

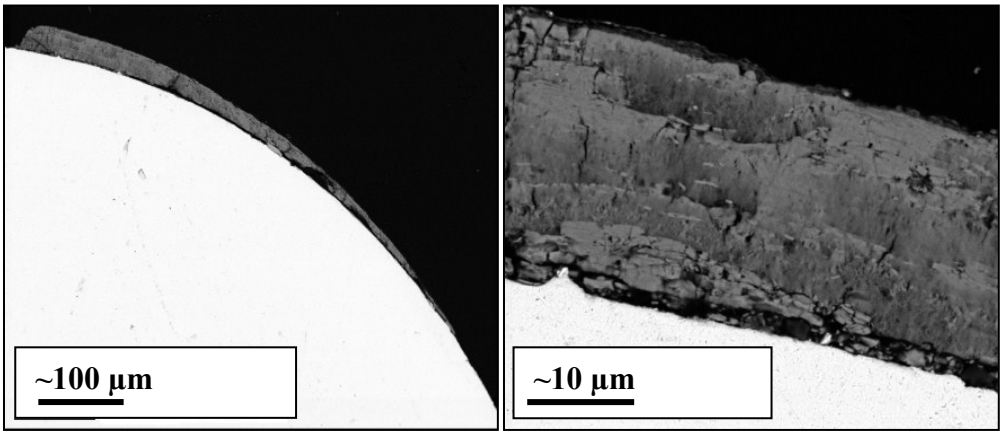

Fig. 50. Tungsten wire x-section (left) with the magnified x-section (right); Experiment 5 - 69 hours at 280°C.

The exact reason for the thicker section of coating on the wire is unknown. Since the wire was not fluidized with the rest of the microspheres, it could have developed a

different boundary layer thickness across the circumference of the wire (Fig. 51). The thinner boundary layer would have a high diffusion coefficient and would grow faster than an area of wire with a thicker boundary layer [18].

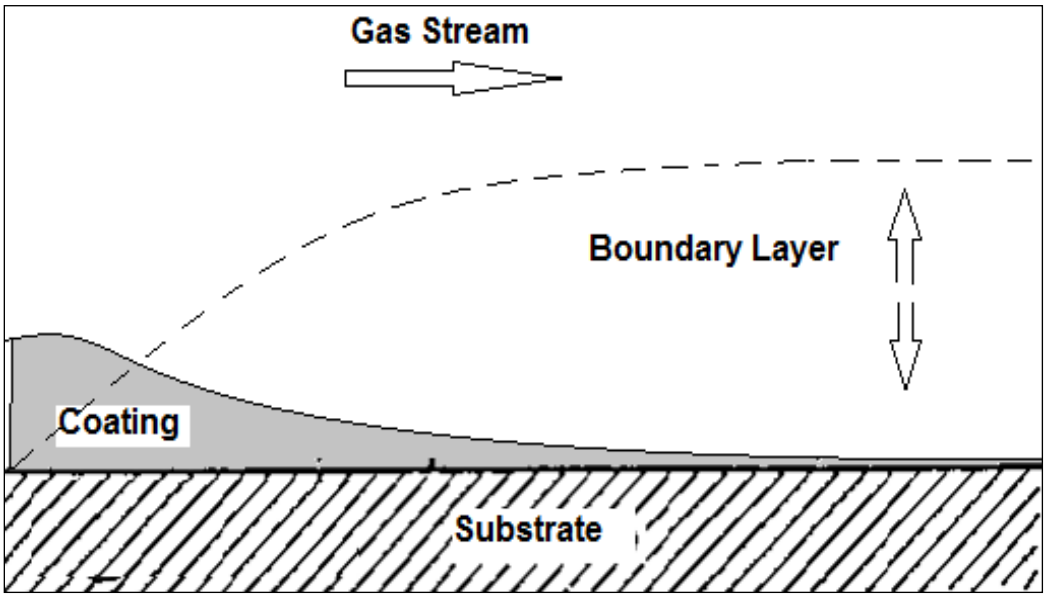

Figure 51. Boundary layer thickness versus coating deposition thickness.

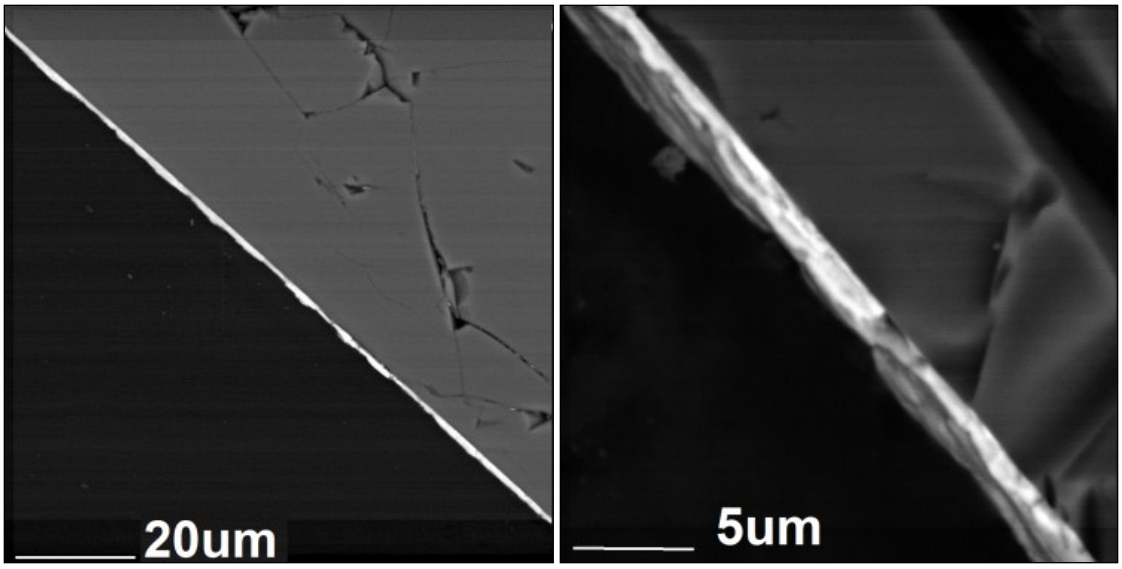

Fig. 52. Reaction vessel x-section (left) with the magnified x-section (right); Experiment 5 - 69 hours at 280°C.

The final BSE image is of the reaction vessel circumference cross section. The BSE image showed an even coating of roughly 2.5 μm around the inner circumference of the reaction vessel (Fig. 52).

The surface of the coated microspheres from experiments 3-5, the ~30 μm tungsten wire coating, and the ~2.5 μm coating on the reaction vessel inner surface were analyzed using WDS methods. The zirconia-silica microspheres are expected to show peaks for silicon, zirconium and oxygen and the WDS plot showing the zirconium content of the surface of the microspheres is provided in Fig 53. A WDS plot comparing the nitrogen content of the bare microspheres is provided in Fig. 54. The WDS analysis for the comparison of the zirconium and nitrogen content of the tungsten wire surface and cross section are provided in Figs. 55 and 56, respectively.

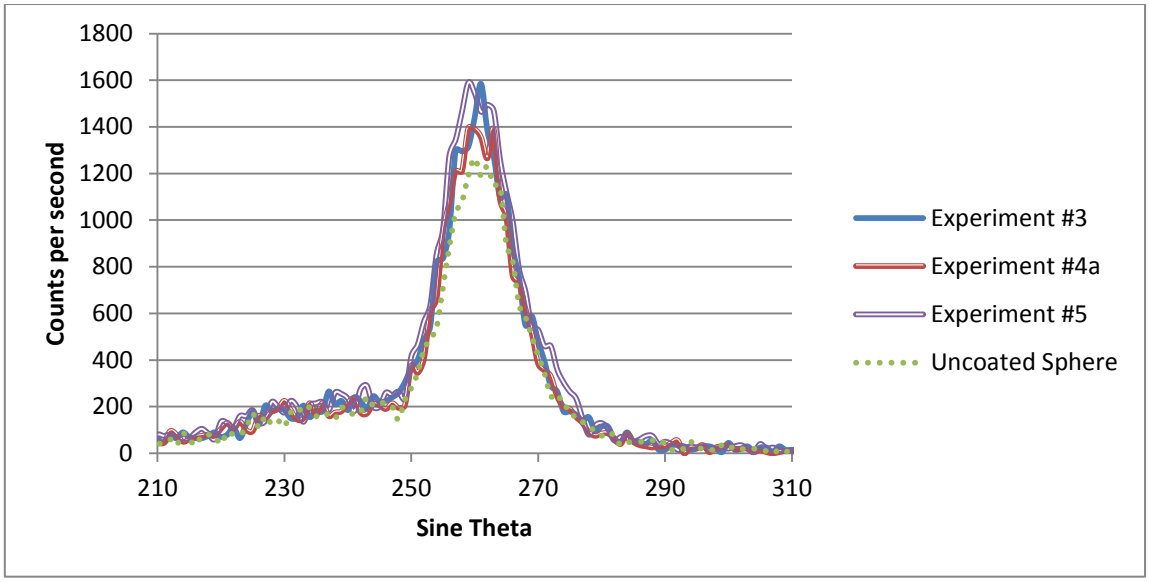

Fig. 53. WDS comparing the zirconium content on the surface of the microspheres.

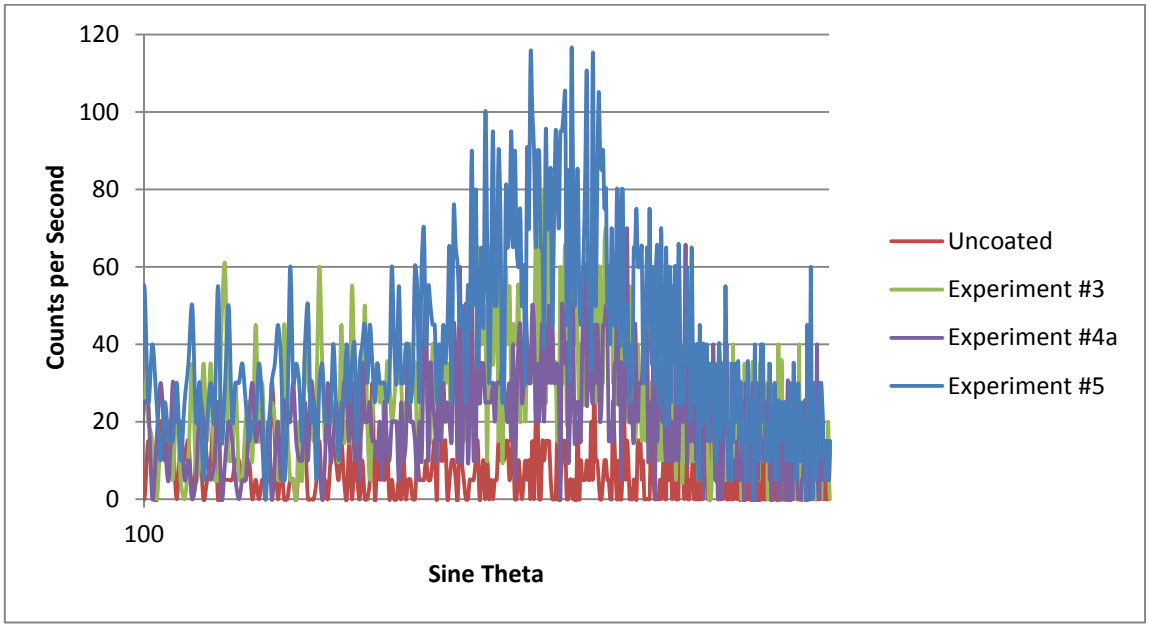

Fig. 54. WDS comparing the nitrogen content on the surface of the microspheres.

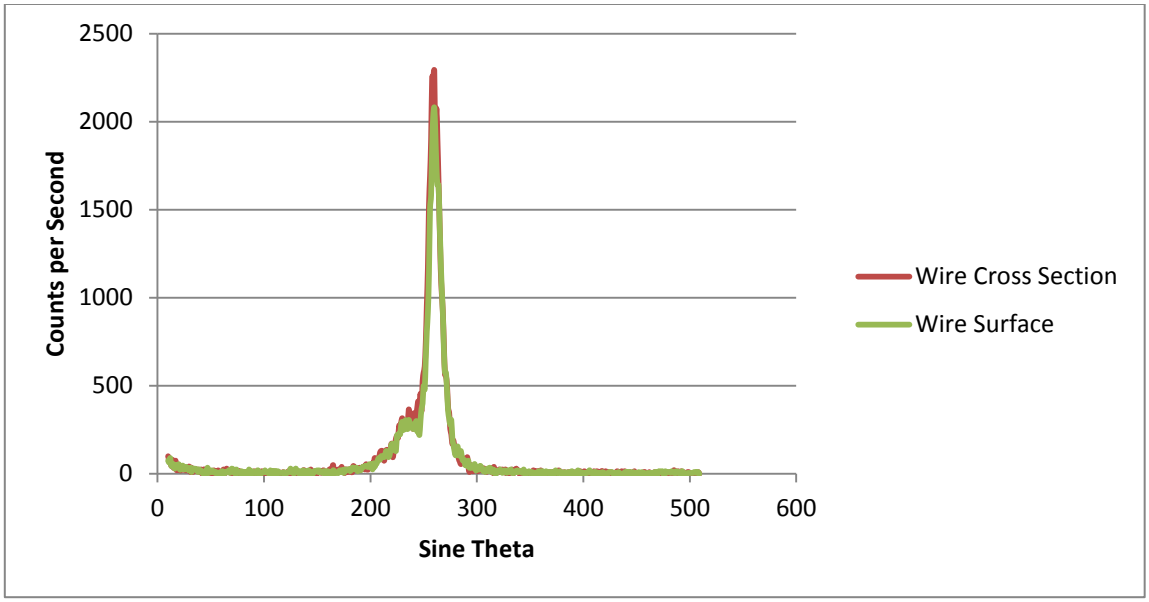

Fig. 55. WDS comparing the zirconium content on the surface of the tungsten wire.

X-ray maps of the contents of each of the coatings for experiments 3 to 5 are discussed next. The carbon map is included in each figure, but the results are inconclusive since each sample is carbon coated before placement in the EPMA. Figures 56, 57, and 58 are the x-ray maps for microsphere experiments 4a, 3, and 5 respectively. The most interesting is the experiment 5 map, the image clearly shows the concentrations of zirconium and nitrogen are higher in areas with little silicon and oxygen. The silicon and oxygen are areas of no or very little coating.

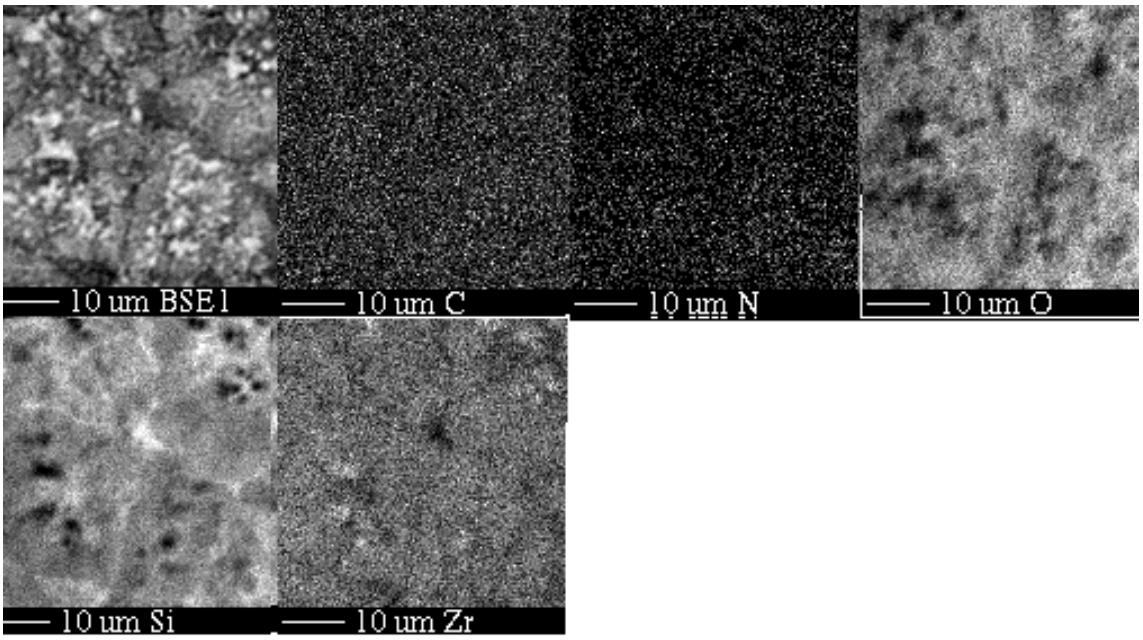

Fig. 56. Experiment 4a x-ray map.

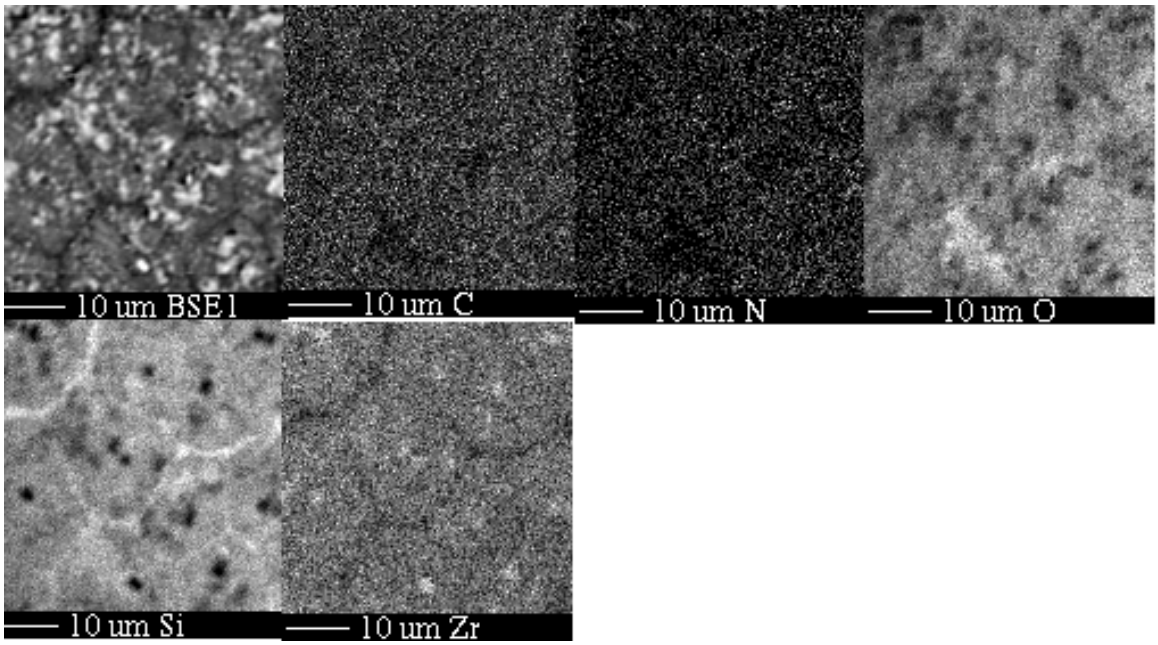

Fig. 57. Experiment 3 x-ray map.

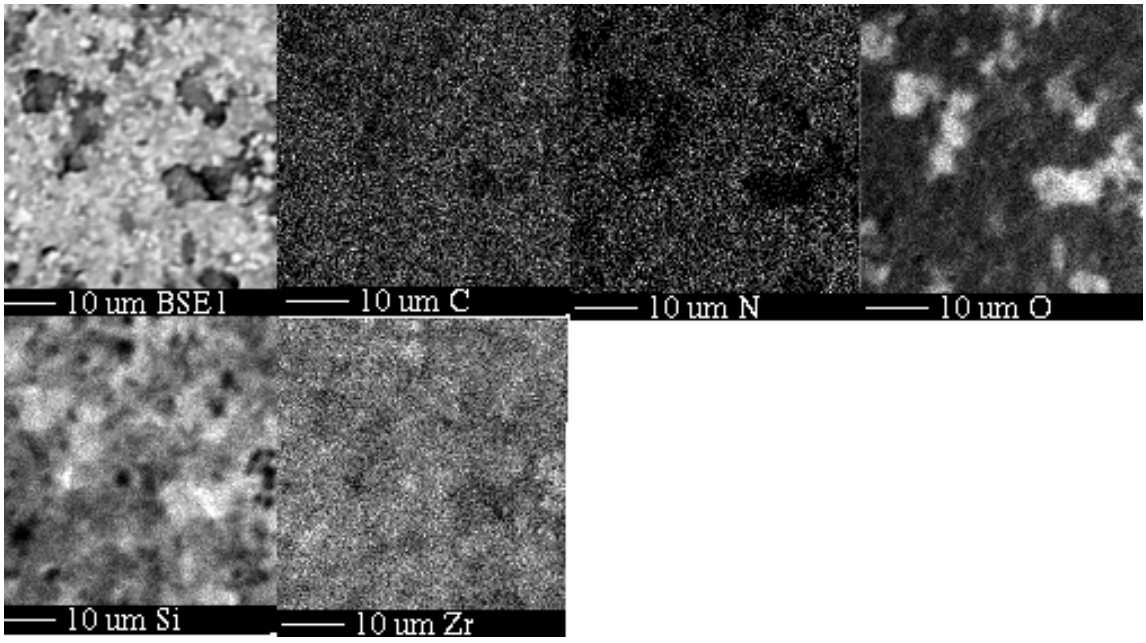

Fig. 58. Experiment 5 x-ray map.

The final x-ray maps to present are from the tungsten wire surface and tungsten wire cross section in Figs. 59 and 60. The image in Fig. 60 has even concentrations over the cross sectional area of nitrogen, oxygen and zirconium in each map, showing a more homogeneous coating than found on the microspheres. There was little nitrogen found on the wire coating, most of the coating consists of zirconium and oxygen.

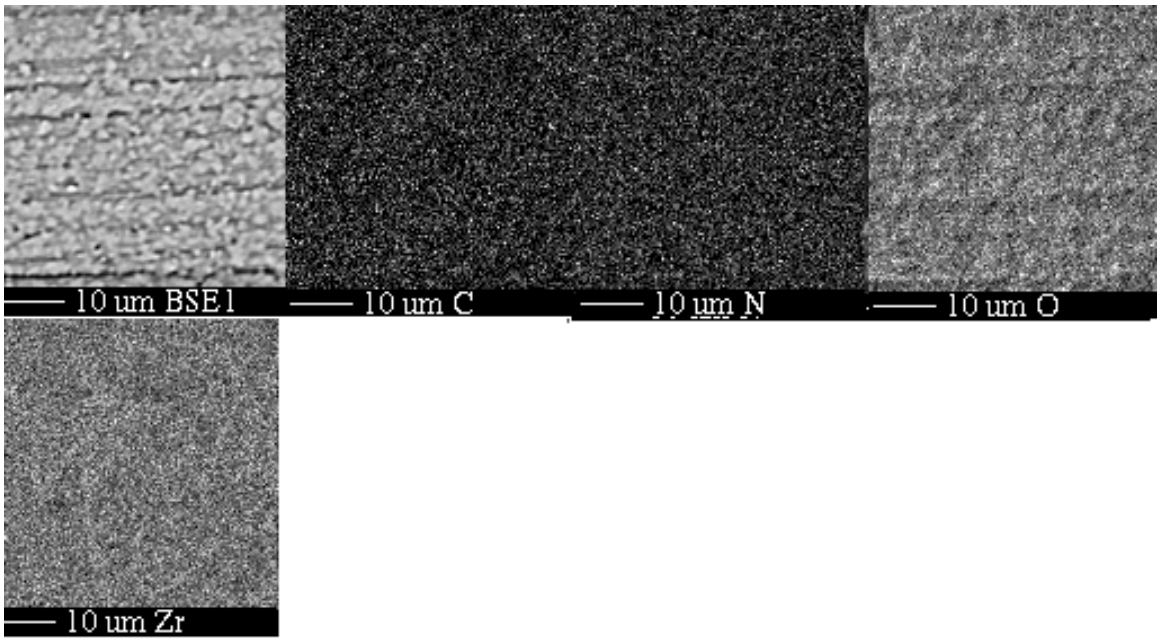

Fig. 59. Experiment5 tungsten wire surface x-ray map.

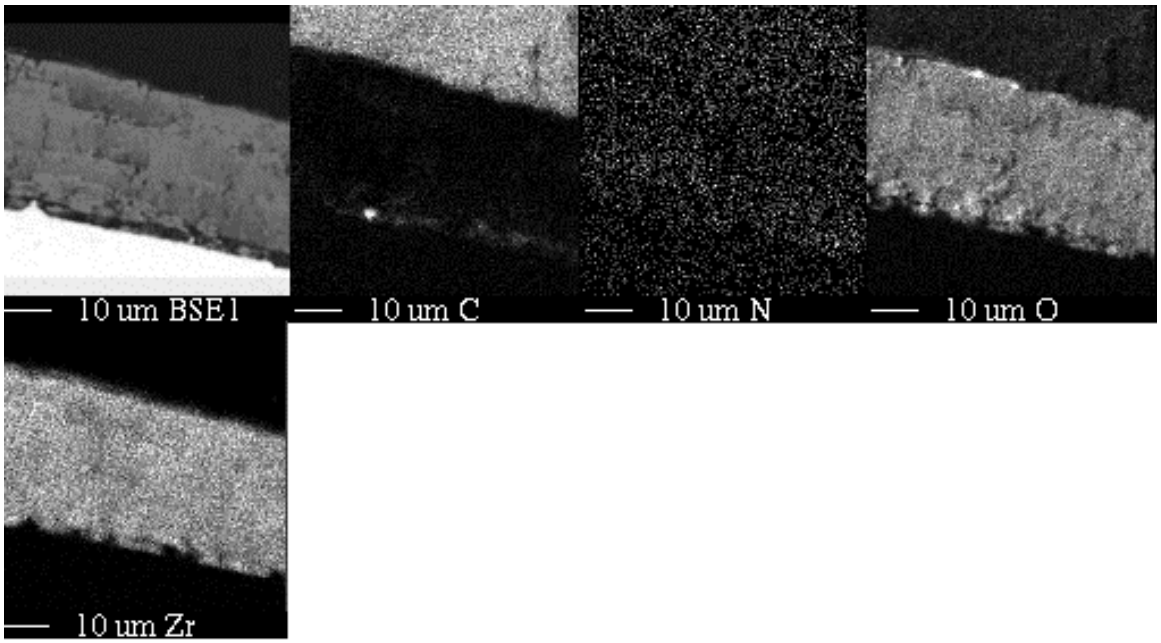

Fig. 60. Experiment 5 tungsten cross section surface x-ray map.

4.4.8 Inverted Fluidized Bed Results Summary

Chemical vapor deposition of zirconium based coatings was achieved without the use of ammonia in the Section 4.4 experiments. The results from Section 4.4.2 indicate that the inclusion of ammonia with the precursor gas flow in the reaction vessel inhibits the coating process.

The white color of the zirconia-silica microspheres facilitated visual coating inspections prior to sample examination at the EPMA but uniform coatings were not obtained using this material as a substrate surrogate. Uniform coatings and even element distributions were observed on the tungsten wire and the reaction vessel surfaces, indicating that although the zirconia-silica microspheres are not an optimal surrogate for the coating process, another powder substrate material can be used to optimize the CVD process.

Heating the TDMAZ precursor below the melting point apparently slowed the precursor decomposition process. Although the precursor was not completely consumed with the Section 4.4 experiments, the discoloration of the precursor crystals was no longer observed at the conclusion of each experiment operation. Bubbler evaporation methods have proven inefficient for the vaporization of this precursor at atmospheric pressure.

The inverted fluidized bed reactor (Section 3.2) was successfully used for the Section 4.4 experiments. The powder substrate was transported within the vessel and the reaction vessel was incorporated into the experiment system without any vessel fractures or mechanical failures. The powder substrate was fluidized during system operation

without any particle entrainment in the carrier gas flow. The precursor vapor was successfully transported within the inverted vessel to the heated reaction zone where the chemical reaction was initiated on the heated particles.

5. DISCUSSION OF RESULTS

Section 5.1 will focus on the results from the fluidized bed reaction vessels and the particulate substrates utilized. Section 5.2 provides discussion of the CVD process including precursor evaporation and particulate substrate choice.

5.1 Fluidization Discussion

5.1.1 Fluidized Bed Reaction Vessel

The spouted fluidized bed reaction vessel successfully fluidized particles of varied size, shape, and density as reported in Section 4.1.2. However, problems were encountered with this design, which included over fluidization and under fluidization of the particulate substrates and frequent vessel fractures during assembly and disassembly.

Over-fluidization was encountered when differences in size distribution and shape within each particle loading required higher and/or lower minimum fluidization velocities: smaller particles invariably were carried from the reaction vessel to the particle trap over the operation of each fluidization experiment. Pronounced over-fluidization apparently occurred as a result of temperature changes during the operation of the system; the increased viscosity of the gas may have decreased drag on the particles, which in turn reduced the minimum fluidization velocity. Particles were carried out of the reaction vessel and regular manual changes in the argon mass flow rates were needed to preserve the fluidized particle bed.

The particles fluidized lower than the conical portion of the reaction vessel in each fluidization experiment with the spouted FB vessel design. Increasing the mass flow rate of the argon gas would raise the fluidization height of the particle bed, but would cause more particles to fluidize out the exhaust line at the top of the vessel.

One solution to overcome this problem would be to increase the diameter and height of the reaction vessel, while leaving the inlet diameter the same size. The increase in the vessel diameter would increase the pressure drop over the length of the reaction vessel and would slow the velocity of the particles before they could exit the top of the vessel. However, the furnace inner diameter was 7.62 cm (3 in), restricting the maximum outer diameter of the reaction vessel.

The fragility of the reaction vessel led to unavoidable cracks and fractures where the vessel gas inlet and outlet lines attached to the stainless steel tubing. The frequent breakage of the vessel delayed subsequent experiment operation while repairs were completed.

The solution to the problems above was the redesign of the vessel into an inverted fluidized bed. The new design was mostly stainless steel; in particular all gas inlets/outlets were made from stainless steel. The glass tube was easily removed during loading, cleaning, and storage. The vessel was compact and could be transported to and from the glovebox with the substrate sealed inside the vessel.

Particulate fluidization experiments within the inverted fluidized bed reaction vessel were successful. Particles remained fluidized in the fluidization tests and system

operation experiments reported in Section 4.4 without any losses to the particle trap attached to the exhaust line. This design can be easily scaled for larger particle loadings.

5.1.2 Particulate Fluidization

The fluidization experiments for varied particle sizes, shapes and densities required minimum mass flow rate values close to the calculated values in Section 4.1.1. The mass flow rate required to keep the particle bed fully expanded during experiment operation deviated from the predicted values from the calculations as well as the initial fluidization experiments.

The fluidization calculations as well as the initial fluidization experiments used only argon as the fluidization gas. Fluidization during system operation was achieved using ammonia and the TDMAZ vapor mixed with the argon gas. The partial pressure of the individual gases will impact the required fluidization velocity as each gas has significantly different fluid properties over the operation range of the system. The partial pressures of each individual gas will directly impact the minimum fluidization velocity for the system.

The shape factor used to classify the zirconia-silica and the U-7Mo particles provided a close estimate for the fluidization requirements. The shape factor estimate used for the tungsten particles did not provide as accurate calculations. The tungsten particle shape deviates from a perfect sphere; some particles were flat and the powders would agglomerate to form larger clumps. The tungsten particles were fluidized in the spouted bed system discussed in Section 4.1, but over a period of time, clusters of the

particles would over-fluidize or drop from the particle bed. The irregular shape of the particles and agglomerates would change the required mass flow to fluidize the particles within the gas stream depending on whether the majority of the surface area was perpendicular or parallel to the gas flow. The particles were successfully fluidized within the inverted fluidized bed but some smaller, irregularly shaped particles were fluidized out of the intended heated area towards the top of the vessel. Particles that fluidize out of the reaction zone will not be uniformly coated like the particles that remain with the heated reaction zone. FB-CVD reactors appear best suited for sphere-shaped particulate substrates.

5.2 Chemical Vapor Deposition Results

The inverted FB-CVD system achieved thin zirconium-bearing coatings on the substrates used in the Section 4.4 experiments. Different types of coatings were achieved in experiment 5 depending on the substrate used; the coatings produced on the zirconia-silica microspheres were adherent, porous, and varied in concentration across the surface and the coatings produced on the reaction vessel were adherent with a uniform coating thickness and even element concentration across the surface. The final coating on the reaction vessel found with BSE imaging in Section 4.4.7, achieved after 69 hours of system operation time, was adherent, roughly 2.5 μm in thickness, and uniform across the vessel surface. Assuming a constant precursor delivery to the substrate surface, this would equal a coating deposition rate of 0.04 ± 0.02 μm/hour.

This coating rate is significantly low compared to deposition rates reported of up to 0.76 μm/hour by W.-I. Kim et al. [18].

5.2.1 Coating Impurities

Zirconium being a refractory metal has a high affinity for oxygen. The formation of an oxide layer in the film is expected even in a vacuum environment (10^{-4} Pa) [15]. The oxygen impurities in the system can be attributed to oxygen absorbed on the inside reaction vessel surface, oxygen present in the process gases, or possible leaks in the experiment system.

Research concerning the metallo-organic precursor for zirconium and titanium indicates that carbon impurities should be expected with the use of the metallo-organic precursor. The ligands directly bound to the ZrN molecule may not completely separate from the molecule during the chemisorption reaction on the substrate surface and can be then incorporated into the growing film. Decomposition reactions occurring prior to or during the deposition process could also lead to the carbon atoms directly binding to the zirconium metal atom (ZrC) adding further impurities to the coating [11, 14-16, 28].

Ammonia is introduced to the MOCVD system to reduce the carbon impurities through a series of transamination reactions [27]. The process is described by R. Fix et al. in Eq. (9).

$$N(NR_2)_4 + NH_3 \rightarrow M(NR_2)_{4-n}(NH_2)n + nHNR_2 \qquad \text{Eq. (9) [28]}$$

where for the case of the TDMAZ precursor, R=CH_3 and M=Zr.

Ammonia can react with the TDMAZ precursor to form a powder even at low temperatures [28]. This reaction was observed to have occurred in the U-7Mo experiments of Section 3.2, when the ammonia was mixed with the vaporized precursor prior to entering the reaction chamber and a yellow powder was evident in the exhaust gas lines; however this parasitic reaction was not observed in the first set of experiments with the molybdenum and tungsten wire in Section 3.1. During the experiments in Section 3.1, the ammonia mass flow controller began to malfunction, with the digital readout from the device rapidly changing between high and low values. Discussion with a technician from the manufacturer suggests that the ammonia mass flow controller may never have functioned during the course of the experiments or if flow was produced from the mass flow controller it could have been sporadic, intermediate bursts. This indicates that the coatings described in Section 3.1 may have been achieved without the presence of the ammonia in the system.

5.2.1 Precursor Evaporation

The coating rate reported in section 5.2 is limited by the vapor delivery of the TDMAZ precursor. All experiments from Section 4 failed to fully evaporate the precursor during the operation of the experiment; therefore the low deposition rate cannot be categorized as a diffusion rate limited reaction or a surface-kinetics rate limited since excess reactants were never present on the substrate surface.

The use of the TDMAZ precursor at atmospheric pressure proved challenging over the course of this research. The vapor pressure of the TDMAZ was too low to

obtain a reliable vaporization rate or partial pressure calculation of the precursor. The fluidized bed experiments were all open system processes and the system pressure could not be reduced to increase the vaporization of the precursor. Heating the precursor for an extended period of time higher than the melting point appeared to reduce the vaporization of the precursor, indicating that possible decomposition reactions were occurring during heating and changing the nature of the precursor. The method used to overcome this in this work (Section 4.4) was to heat the precursor below the melting point of the crystals to increase the vaporization and slow the decomposition process. This is far from an optimal solution as the last experiment completed for this research operated for a total of 69 hours and a large amount of the precursor remained in the precursor bubbler. A more efficient delivery system needs to be implemented for the TDMAZ precursor so that accurate coating deposition rates may be calculated.

5.2.2 Substrate Dependent Coatings

The experiments from Section 4.4 had different results depending the on the substrate utilized. The coatings on the porous zirconia-silica microspheres were inhomogeneous and nucleated from specific areas on the microsphere surface. The coating on the tungsten wire appeared more uniform, but the thickness varied around the circumference as a result of its stationary position within the reaction vessel. The coating around the Pyrex reaction vessel was uniform and homogenous in composition. The irregularity of the coating on the zirconia-silica microspheres suggests that either the varied porosity of the surface changed the coating thickness across the sphere surface or

the surface free energy varied over the different compositions found on the microsphere surface. Both conclusions suggest that the zirconia-silica microspheres were not an optimal choice as a particulate surrogate in the CVD experiments from the perspective of surface reactions, although it was a functional choice for fluidization and visual coating inspections.

6. SUMMARY AND RECOMMENDATIONS

The FB-CVD system utilizing a metalorganic precursor at low deposition temperatures and atmospheric pressures successfully deposited zirconium based coatings onto zirconia-silica microspheres. Resultant coatings had significant oxygen contamination and possible carbon contamination. Adjustment to system parameters as well as modification to the precursor evaporation must be further researched. The following recommendations are made if research using the inverted FB-CVD reactor is to continue:

1. The precursor delivery system must be improved. The vapor pressure of the solid TDMAZ precursor is too low at atmospheric pressure to utilize a traditional bubbling system, (i.e., only ~10% of the precursor inserted into the bubbler is utilized with each experiment). Although other delivery methods are much more expensive, it will be more cost effective to utilize the entire precursor loaded in each experiment run. Knowing the amount of precursor vaporized will also enable calculations of vaporization rate and subsequently coating deposition rate on the microspheres.

2. Once a constant precursor vapor pressure is supplied, a parametric study of the operating temperature of the system should be completed. A CVD system can change from a diffusion rate controlled system to a surface kinetics rate

controlled system depending on the substrate temperature. The MOCVD experiment in literature [8] is operated at lower temperatures since the substrate is within an ultra-low pressure environment. Increasing the temperature will increase the coating deposition rate [11] and will decrease the carbon contamination found in thin film deposition processes utilizing the metallo-organic precursors [11, 14-16, 28]. This will need to be optimized however since the coating rate peaks and then decreases with increased temperature as parasitic gas phase reactions are more probable with higher temperatures [8]. With a new precursor delivery system, a parametric study can be made to optimize the substrate temperature for the desired coating composition and thickness.

Reduction of the oxygen contamination can be achieved as follows:

1. Oxygen traps and moisture traps should be attached to the gas lines before the low flow inlet to the precursor evaporation system and on the high argon mass flow line prior to entry into the reaction vessel.
2. The FB-CVD system should be relocated into an inert atmosphere glovebox. Disconnecting and reconnecting system components and moving the bubbler and reaction vessel from the inert atmosphere glovebox to the hood where the system was assembled introduces impurities into the experiment during operation. The system would not require the extended purge and heat periods if it was operated and stored within an inert atmosphere.

REFERENCES

[1] DOE, Highly Enriched Uranium: Striking a Balance, A Historical Report on the United States Highly Enriched Uranium Production, Acquisition and Utilization Activities from 1945 through September 30, 1996, Washington, DC: U.S. Department of Energy, http://www.fas.org/sgp/othergov/doe/heu/striking-lofi.pdf , (2001).

[2] D.M. Wachs, RERTR Fuel Development and Qualification Plan, DE-AC07-05ID14517, Idaho National Laboratory, (2007).

[3] V.P. Sinha, P.V. Hegde, G.J. Prasad, G.K. Dey, H.S. Kamath, Effect of Molybdenum Addition on Metastability of Cubic γ-Uranium, Journal of Alloys and Compounds, 491 (2010), pp. 753-760.

[4] G.L. Hoffman, A Short Note on High Density Dispersion Fuel, Argonne National Laboratory (1996).

[5] Y. S. Kim, G.L. Hofman, Irradiation Behavior of the Interaction Product of U-Mo Fuel Particle Dispersion in an Al Matrix, Journal of Nuclear Materials, 425 (2012), pp. 181-187.

[6] A. Leenaers, S. Van den Berghe, E. Koonen, C. Jarousse, F. Huet, M. Trotabas, M. Boyard, S. Guillot, L. Sannen, M. Verwerft, Post-irradiation Examination of Uranium–7wt% Molybdenum Atomized Dispersion Fuel, Journal of Nuclear Materials, 335 (2004), pp. 39-47.

[7] D. D. Keiser, Jr., Evaluation of Ceramic Coatings for Possible Application as a Diffusion Barrier in U-Mo Dispersion Fuel Plates, Idaho National Laboratory, May 2010.

[8] M. Chotirach, S. Tantayanon, S. Tungasmita, K. Kriausakul, Zr-Based Intermetallic Diffusion Barriers for Stainless Steel Supported Palladium Membranes, Journal of Membrane Science, 405–406, (2012), pp. 92-103

[9] M.-A. Nicolet, Diffusion Barriers in Thin Films, Thin Solid Films, 52 (1978), pp. 415-443.

[10] K.-T. Rie, J. Whole, A. Gebauer, Synthesis of Thin Coatings by Plasma-Assisted Chemical Vapour Deposition using Metallo-Organic Compounds as Precursors, Surface and Coatings Technology, 59 (1993), pp. 202-206.

[11] K. T. Rie, A. Gebauer, Plasma-Assisted Chemical Vapour Deposition of Hard Coatings with Metallo-Organic Compounds, Materials Science and Engineering, A139, (1991), pp. 61-66.

[12] Y. Pauleau, Chemical Physics of Thin Film Deposition Processes for Micro- and Nano-Technologies, Kluwar Academic Publishers, Boston, 2002.

[13] Y. Xu, X.-T. Yan, Chemical Vapor Deposition, An Integrated Engineering Design for Advanced Materials, Springer-Verlag, New York, 2010.

[14] H.O. Pierson, Handbook of Chemical Vapor Deposition (CVD) - Principles, Technology and Applications (2nd Edition), Elsevier Science, 2000.

[15] C. B. Alcock, Thermochemical Processes: Principles and Models, Elsevier Butterworth-Heinemann, 2001.

[16] L. Dubois, Model Studies of Low Temperature Titanium Nitride Thin Film Growth, Polyhedron, 13, (1994), pp. 1329-1336.

[17] I.-W. Kim, S.-J. Kim, D.-H. Kim, H. Woo, M.-Y. Park, S.-W. Rhee, Fourier Transform Infrared Spectroscopy Studies on Thermal Decomposition of Tetrakis-dimethyl-amido Zirconium for Chemical Vapor Deposition of ZrN, Korean Journal of Chemical Engineering, 21, (2004), pp. 1256-1259.

[18] Y. Kumashiro, K. Inagawa, Electric Refractory Materials: Thin Film Preparation, Marcel Dekker, Inc., 2000.

[19] H. Berndt, A.-Q. Zeng, H.-R. Stock, P.Mayr, Zirconium, Carbonitride Films Produced By Plasma-Assisted Metal Organic Chemical Vapour Deposition, Surface and Coatings Technology, 74-75 (1995), pp. 369-374.

[20] L.G. Gibilaro, Fluidization Dynamics: The Formulation and Applications of a Predictive Theory for the Fluidized State, Butterworth-Heinemann, Woburn, 2001.

[21] D. Kunii, O.Levenspiel, Fluidization Engineering, Butterworth-Heinemann, Newton, MA, 1991.

[22] W-C. Yang, Handbook of Fluidization and Fluid-particle Systems, Marcel Dekker, 2003.

[23] A. Lucas, J. Arnaldos, J. Casal, L. Pulgjaner, Improved Equation for the Calculation of Minimum Fluidization Velocity, Industrial and Engineering Chemistry Process Design and Development, 25 (1986), pp. 426-429.

[24] W.E. McCabe, J.C. Smith, P. Harriott, Unit Operations of Chemical Engineering, McGraw Hill, New York, 2001.

[25] Deep Crust & Mantle Dynamics Group, Research Facilities: Electron Microprobe Laboratory, http://www.dcmd.tamu.edu/research-facilities.

[26] Goodge, J., Geochemical Instrumentation and Analysis: Electron probe micro-analyzer (EPMA), University of Minnesota-Duluth, http://www.serc.carleton.edu/research_education/geochemsheets/techniques/EPMA.html, February 2012.

[27] Strem Chemicals, Inc., Material Safety Data Sheet; Tetrakis(dimethylamino)zirconium, 99% TDMAZ, http://www.strem.com, January 2011.

[28] NIST: Thermophysical Properties of Fluid Systems, (2012). http://www.webbook.nist.gov/chemistry/fluid/, January 2011.

[29] H. Guillon, S. Bonnafous, Vaporization of Solid or Liquid Organic, Organometallic or Inorganic Compounds, Gases & Instrumentation, May 2008.

[30] R. Fix, R. G. Gordon, D. M. Hoffman, Chemical Vapor Deposition of Titanium, Zirconium, and Hafnium Nitride Thin Films, Journal of Chemical Materials, 3 (1991), pp. 1138-1148.

VITA

Name:	Marie Arrieta
Address:	Sandia National Laboratories MS 1377, 10600 Research Rd., Albuquerque, NM 87123
Email Address:	myarrie@sandia.gov
Education:	B.S., Nuclear Engineering, The University of New Mexico, 2010 M.S., Nuclear Engineering, Texas A&M University, 2012